White Rose
university consortium
Universities of Leeds, Sheffield & York

eprints@whiterose.ac.uk
https://eprints.whiterose.ac.uk/

# Techno-economic Assessment of CO₂ Quality Effect on its Storage and Transport: CO₂QUEST

# An overview of Aims, Objectives and Main Findings

Richard T.J. Porter[a,b], Haroun Mahgerefteh[a,*], Solomon Brown[a,†], Sergey Martynov[a], Alexander Collard[a], Robert M. Woolley[b], Michael Fairweather[b], Samuel A.E.G. Falle[c], Christopher J. Wareing[d], Ilias K. Nikolaidis[e], Georgios C. Boulougouris[e], Loukas D. Peristeras[e], Dimitrios M. Tsangaris[e], Ioannis G. Economou[e], Carlos Salvador[f], Kourosh Zanganeh[f], Andrew Wigston[f], John N. Najalafi[f], Ahmed Shafeen[f], Ashkan Beigzadeh[f], Régis Farret[g], Phillipe Gombert[g], Jerome Hebrard[g], Christophe Proust[g], Anthony Ceroni[g], Yann Flauw[g], Yong Chun Zhang[h], Shaoyun Chen[h], Yu Jianliang[h], Reza H. Talemi[i], Jacob Bensabat[j], Jan Lennard Wolf[k], Dorothee Rebscher[k], Auli Niemi[l], Byeongju Jung[l,‡], Niall Mac Dowell[m,n], Nilay Shah[n], Clea Kolster[n], Evgenia Mechleri[n], Sam Krevor[n]

[a]Department of Chemical Engineering, University College London, London WC1E 7JE, UK, [b]School of Chemical and Process Engineering, University of Leeds, Leeds LS2 9JT, UK, [c]School of Mathematics, University of Leeds, Leeds LS2 9JT, UK, [d]School of Physics and Astronomy, University of Leeds, Leeds LS2 9JT, UK, [e]National Center for Scientific Research "Demokritos", Institute of Nanoscience and Nanotechnology, Molecular Thermodynamics and Modelling of Materials Laboratory, Aghia Paraskevi, Attikis GR–153 10, Greece, [f]CanmetENERGY, Natural Resources Canada, Ottowa, K1A 1M1, Canada, [g]INERIS, Parc Technologique ALATA, Verneuil-en-Halatte BP 2, 60550, France, [h]School of Chemical Engineering, Dalian University of Technology, Dalian, People's Republic of China, [i]ArcelorMittal Global R&D Gent-OCAS NV, Pres. J.F. Kennedylaan 3, 9060 Zelzate, Belgium, [j]Environmental and Water Resources Engineering Ltd, Haifa, Israel, [k]Bundesanstalt für Geowissenschaften und Rohstoffe (BGR), Geozentrum Hannover, Stilleweg 2, 30655 Hannover, Germany, [l]Uppsala University, Department of Earth Sciences, Villavägen 16, SE-75236 Uppsala, Sweden, [m]Centre for Environmental Policy, Imperial College London, London SW7 1NA, UK, [n]Centre for Process Systems Engineering, Department of Chemical Engineering, Imperial College London, London SW7 2AZ, UK.

[†]Current address: Department of Chemical and Biological Engineering, University of Sheffield, Sheffield, London S1 3JD, UK.

[‡]Current address: Division of Earth Environment Research, Korea Institute of Geoscience and Mineral Resources, Daejeon 305-350, South Korea.

[*]Corresponding author and CO₂QUEST Project Coordinator: Tel: +44(0)207 679 3835

Email address: H.Mahgerefteh@ucl.ac.uk (Haroun Mahgerefteh).

**Submission of a full-length article to the International Journal of Greenhouse Gas Control, of unpublished material not submitted for publication elsewhere**

# ABSTRACT

This paper provides an overview of the aims, objectives and the main findings of the $CO_2$QUEST FP7 collaborative project, funded by the European Commission designed to address the fundamentally important and urgent issues regarding the impact of the typical impurities in $CO_2$ streams captured from fossil fuel power plants and other $CO_2$ intensive industries on its safe and economic pipeline transportation and storage. The main features and results recorded from some of the unique test facilities constructed as part of the project are presented. These include an extensively instrumented realistic-scale test pipeline for conducting pipeline rupture and dispersion tests in China, an injection test facility in France to study the mobility of trace metallic elements contained in a $CO_2$ stream following injection near a shallow-water qualifier and fluid/rock interactions and well integrity experiments conducted using a fully instrumented deep-well $CO_2$/impurities injection test facility in Israel. The above, along with the various unique mathematical models developed, provide the fundamentally important tools needed to define impurity tolerance levels, mixing protocols and control measures for pipeline networks and storage infrastructure, thus contributing to the development of relevant standards for the safe design and economic operation of CCS.

**Dedication:** This paper is dedicated to the memory of our friend and colleague, Dr. Robert M. Woolley, who made a significant input to the $CO_2$QUEST project and whose expertise, commitment and support inspired many of those around him.

## KEYWORDS

CCS, CCS cost/benefit analysis, CCS safety, $CO_2$ impurities, multi-phase flow, mathematical modelling.

# 1. INTRODUCTION

For large-scale applications of $CO_2$ Capture and Storage (CCS), transport of $CO_2$ using high pressure pipelines is found to be the most practical and economic method (Serpa et al., 2011). However the $CO_2$ stream captured from fossil fuel power plants or other $CO_2$ intensive industries will contain a range of different types of impurities each having its own impact on the different parts of the CCS chain. Such impurities may be classified broadly by origin into three main categories arising from fuel oxidation, excess oxidant/air ingress, and process fluids as shown in Table 1 (Porter et al., 2015). Water is a major combustion product and is considered an impurity in the $CO_2$ stream. The elements inherently present in a fuel such as coal include sulfur, chlorine and mercury, and are released upon complete or incomplete combustion and form compounds in the gas phase which may remain to some extent as impurities in the $CO_2$ after it is captured and compressed. The oxidising agent used for combustion, such as air, may result in residual impurities of $N_2$, $O_2$ and Ar; these same impurities may also result from any air ingress into the process. The materials and chemicals used for the $CO_2$ separation process, such as monoethanolamine (MEA) used for post-combustion capture, or Selexol in pre-combustion capture, and their degradation products can be carried over into the $CO_2$ stream constituting a further class of impurity.

**Table 1.** Classes of potential $CO_2$ impurities by origin.

| Coal/biomass oxidation products | |
|---|---|
| Complete | Partial |
| $H_2O$, $SO_X$, $NO_X$, HCl, HF | CO, $H_2S$, COS, $NH_3$, HCN |
| Volatiles | Biomass alkali metals |
| $H_2$, $CH_4$, $C_2H_6$, $C_3$+ | KCl, NaCl, $K_2SO_4$, KOH etc. |
| Trace metals | Particulates |
| Hg ($HgCl_2$), Pb, Se, As etc. | Ash, PAH/soot |
| **Oxidant / air ingress** | **Process fluids** |
| $O_2$, $N_2$, Ar | Glycol, MEA, Selexol, $NH_3$ etc. |

Impurities that arise from $CO_2$ capture sources can have a number of important impacts on the downstream transport and storage infrastructure and operation. The presence of impurities in $CO_2$, such as air derived non-condensable species ($N_2$, $O_2$ and Ar), can shift the dew point and bubble point lines on the mixture phase diagram to higher pressures compared with pure $CO_2$. As a result higher operating pressures will be needed to keep $CO_2$ in the dense phase, thus impacting on compression and transport costs. In addition, these species can reduce the

CO$_2$ structural trapping capacity in geological formations by a greater degree than their molar fractions (Wang et al., 2012). Hydrogen may be present in pre-combustion capture derived CO$_2$ streams, introducing the risk of embrittlement of the pipeline steel. Additionally, hydrogen significantly affects the rate of inventory pressure loss during pipeline transportation of CO$_2$ (Wetenhall et al., 2014). Enhanced Oil Recovery applications require stricter limits, particularly on O$_2$ due to its promotion of microbial growth and reaction with hydrocarbons. Water should be limited in CCS applications in order to avoid corrosion arising from the formation of in situ carbonic acid (Cole et al., 2011) along with clathrate formation and condensation (Serpa et al., 2011). Conversely, water may be of benefit even at high concentrations in storage given its immobilisation effect on CO$_2$.

Sulfur species (H$_2$S, COS, SO$_2$ and SO$_3$) may pose a corrosion risk in the presence of water and there are additional toxicity concerns for H$_2$S. NO$_X$ species may be present in CO$_2$ streams as combustion by-products, posing a corrosion risk due to nitric acid formation (Sim et al., 2013). Trace elements such as Lead, Mercury and Arsenic in the CO$_2$ stream are of concern for geological storage due to their toxicity and the possibility that they could contaminate groundwater. Amongst the numerous potential trace metal CO$_2$ impurities, mercury receives further attention for its corrosive effects on a number of metals. Due to its toxicity, limits are also suggested for carbon monoxide. For other components that may be present in CO$_2$ streams (e.g., HCl, HF, NH$_3$, MEA, Selexol), not enough information is available to fully understand their downstream impacts on transport and storage and thus determine maximum allowable amounts. Further work is therefore required to understand the impacts of these species in transport and storage applications and to elucidate potential crossover effects.

In CCS systems, capture costs can be expected to increase with increasing CO$_2$ purity as additional process unit operations and the increased energy penalty associated with achieving purer CO$_2$ is taken into consideration. Conversely, transport and storage costs (per tonne of CO$_2$ transported) may be expected to decrease with increasing CO$_2$ purity due to the lower compression requirements to keep CO$_2$ in the dense phase, lower rates of corrosion and the relaxation of safety measures needed to deal with hazardous impurities. When capital and operating costs are factored together to calculate a levelised "total cost" for CCS systems a minima for a given purity and composition range is expected where the system may be assumed to be cost optimised in addition to having the necessary safety precautions

implemented. The challenge therefore is to find the optimum range and concentration of impurities that can be permitted in a $CO_2$ stream to enable its safe and cost-effective transportation and storage.

The $CO_2QUEST$ project addresses the fundamentally important issues surrounding the impact of the typical impurities in $CO_2$ streams derived from fossil fuel power plants or other $CO_2$ intensive industry on the safe and economic transportation and storage of $CO_2$. Based a techno-economic analysis, $CO_2QUEST$ elucidates the optimum level of $CO_2$ purification required for CCS in consideration of the effects of impurities on pipeline transportation, geological storage and the purification costs with safety and environmental issues being the overarching factors.

This paper describes the objectives, methodology and the main findings of the $CO_2QUEST$ project. Section 2 defines the project's scope and work package structure. Section 3 discusses the fluid properties and phase behaviour of $CO_2$ mixtures, characterising the $CO_2$ stream impurities and determining their physical properties. Sections 4 and 5 cover the impact of $CO_2$ stream impurities on pipeline transportation, compression and storage. The techno-economic methodology and risk assessment work is presented in Section 6, followed by Conclusions in Section 7.
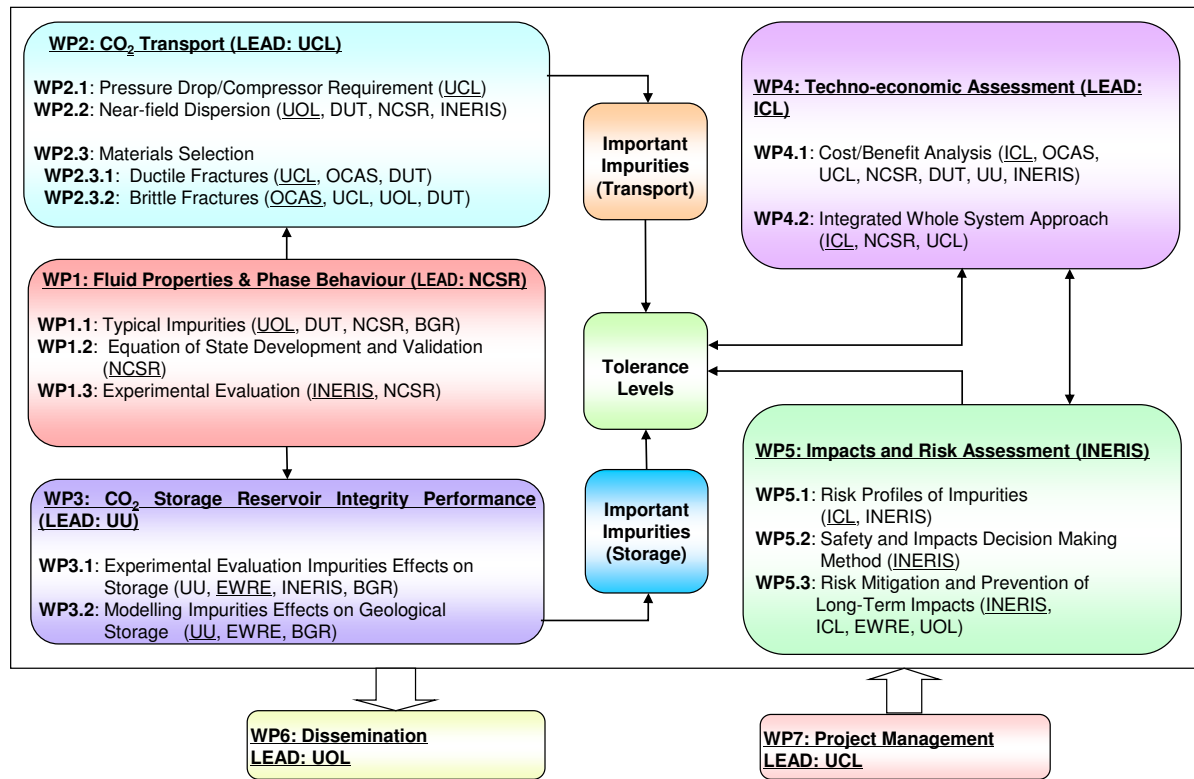
# 2. PROJECT WORKPACKAGES



**Figure 1.** Pert diagram representation of the CO$_2$QUEST project structure.

Figure 1 presents the CO$_2$QUEST project structure in the form of various Work Packages (WPs) along with their interactions. The following sections provide summary descriptions of the aims, objectives and main findings of each WP.

# 3. WP1 – FLUID PROPERTIES AND PHASE BEHAVIOUR

## 3.1    Typical impurities and cost-benefit analysis

The work in this section, based on literature studies, underpins the other project activities by providing analysis of the ranges and levels of impurities present in $CO_2$ streams derived from different carbon capture sources, including those from both the power sector and heavy industries. The factors that affect the ranges and levels of impurities for given power generation technologies, such as post-combustion, pre-combustion and oxyfuel combustion capture, have also been identified leading to the ranges as set out in Table 2.

**Table 2.** $CO_2$ impurities from different $CO_2$ capture technologies

|  | Oxyfuel Combustion | | | Pre-combustion | Post-combustion |
|---|---|---|---|---|---|
|  | Raw / dehumidified | Double flashing | Distillation | | |
| **$CO_2$ % v/v** | 74.8-85.0 | 95.84-96.7 | 99.3-99.9 | 95-99 | 99.6 – 99.8 |
| **$O_2$ % v/v** | 3.21-6.0 | 1.05-1.2 | 0.0003-0.4 | 0 | 0.015 – 0.0035 |
| **$N_2$ % v/v** | 5.80-16.6 | 1.6-2.03 | 0.01-0.2 | 0.0195 – 1 | 0.045 - 0.29 |
| **Ar % v/v** | 2.3-4.47 | 0.4-0.61 | 0.01-0.1 | 0.0001-0.15 | 0.0011 – 0.021 |
| **$NO_x$ ppmv** | 100-709 | 0-150 | 3-100 | 400 | 20 - 38.8 |
| **$SO_2$ ppmv** | 50-800 | 0-4500 | 1-50 | 25 | 0 - 67.1 |
| **$SO_3$ ppmv** | 20 | - | 0.1-20 | - | N.I. |
| **$H_2O$ ppmv** | 100-1000 | 0 | 0-100 | 0.1 - 600 | 100 – 640 |
| **CO ppmv** | 50 | - | 2-50 | 0 - 2000 | 1.2 - 10 |
| **$H_2S$/COS ppmv** | 0.2 - 34000 | | | | |
| **$H_2$ ppmv** | 20-30000 | | | | |
| **$CH_4$ ppmv** | 0-112 | | | | |

A techno-economic modelling study of power plants with $CO_2$ capture technologies which focusses on process scenarios that deliver different degrees of $CO_2$ stream purity was also carried out in this work package. The three leading $CO_2$ capture technologies for the power sector are considered, namely; oxyfuel combustion, pre-combustion and post-combustion capture. The study uses a combination of process simulation of flue gas cleaning processes, modelling with a power plant cost and performance calculator and literature values of key performance criteria in order to calculate capital costs, operational and maintenance costs, the levelised cost of electricity and $CO_2$ product purity of the considered $CO_2$ capture options (Porter et al., in prep).

For oxyfuel combustion capture, the calculations are based on a 400 MWg retrofitted power station that uses a low sulfur coal and considers three raw $CO_2$ flue gas processing strategies of compression and dehydration only, double flash system purification and distillation

purification. Analysis of pre-combustion capture options is based on new build integrated gasification combined cycle plants with one gas-turbine and a GE entrained-flow gasifier. Integrated physical solvent systems for capturing $CO_2$ and sulfur species were considered in three ways; co-capture of sulfur impurities with the $CO_2$ stream using Selexol$^{TM}$ solvent or separate capture of $CO_2$ and sulfur impurities using either Selexol$^{TM}$ or Rectisol$^®$ solvent systems. Analysis of post-combustion capture plants was made with and without some conventional pollution control devices.

Of the different cases considered, pre-combustion capture with co-capture of impurities and $CO_2$ using Selexol$^{TM}$ offered the lowest cost with a reasonably high purity of $CO_2$ at 97.64 mol%, but high estimated levels of $H_2S$ (at 3974 ppm$_v$) in the captured stream. The most expensive system was pre-combustion capture using Rectisol$^®$ with separate capture of $CO_2$ and sulfur impurities, producing a dry 99.51 mol% pure $CO_2$ stream. The system with the lowest grade of $CO_2$ was oxyfuel combustion capture with compression and dehydration of the raw $CO_2$ stream only, which resulted in 77.69 mol% pure $CO_2$ and with the second lowest cost. The oxyfuel plant with a distillation purification system and a post-combustion capture plant with conventional pollution control devices had the joint highest $CO_2$ purity (99.99 mol%), with the post-combustion capture system estimated to be the cheaper of the two. The calculations performed are of use in further analyses of whole chain CCS for the safe and economic capture, transport and storage of $CO_2$.

## 3.2 Equation-of-state development for $CO_2$ mixtures and supporting vapour liquid equilibrium data

The Vapour – Liquid Equilibrium (VLE) of $CO_2$ mixtures associated with CCS processes has attracted significant attention both in terms of experimental measurements and modelling using macroscopic models such as equations of state (EoS). Nevertheless, a critical part of the design and operation of CCS facilities is the study of solidification phenomena when $CO_2$ mixes with other gases. Relatively little work has been performed to measure and predict the solid-fluid equilibrium (SFE) of these mixtures. $CO_2$ possesses a relatively high Joule–Thomson coefficient, as a result during transport a sudden pipeline depressurization will lead in rapid cooling and potentially very low fluid temperatures (Woolley et al., 2014). Consequently, solid formation may occur. The objective of this work is the application of

solid thermodynamic models of different complexity to model the SFE of pure $CO_2$ and of $CO_2$ mixtures with other compounds, including $N_2$, $H_2$ and $CH_4$.

Three solid thermodynamic models have been coupled with vapour-liquid EoS to model the SFE of pure $CO_2$ and binary mixtures of $CO_2$ with other gases associated with CCS processes. The solid models include an empirical correlation fitted to experimental data at SFE conditions, a model based on thermodynamic integration and an EoS developed for pure, solid $CO_2$. The solid models have been coupled with Peng-Robinson (PR), Soave-Redlich-Kwong (SRK) and Perturbed Chain-Statistical Associating Fluid Theory (PC-SAFT) EoS which are used widely for liquids and gases. Firstly, every model was evaluated to correlate the pure $CO_2$ solid-liquid (SLE) and solid-vapour (SVE) equilibrium. This way the performance of a solid model coupled with different EoS is tested and the agreement between the different models is assessed. Moreover, an accurate description of the SFE behaviour of pure $CO_2$ is a good basis for subsequent two phase and three phase solid-liquid-gas equilibrium (SLGE) mixture calculations. Because of lack of experimental data for two phase SFE for the $CO_2$ mixtures of interest, the performance of the different models has been evaluated on SLGE conditions, and compared to experimental data from literature (Fandiño et al., 2015; Davis et al., 1962).

The modelling results have shown that a model that successfully reproduces the pure $CO_2$ triple point will more accurately predict the SLG locus of the mixture. In this context, the thermodynamic integration model and the Jäger and Span (2012) EoS provide, in general, more accurate predictions of the SLGE for the mixtures of $CO_2$ with $N_2$ and $H_2$when all binary interaction parameters (BIPs) are zero. For these two mixtures, the empirical correlation model for the solid phase is comparable to the other two models only when coupled with PC-SAFT, which accurately reproduces the pure $CO_2$ triple point. The use of BIPs, regressed from binary VLE data at low temperature, significantly improves the prediction of the SLG behaviour for most models. All models provide very similar results for the $CO_2 - CH_4$ mixture and very low deviations from experimental data have been achieved with the use of BIPs regressed from binary VLE data over a wide temperature range. A representative example is shown in Figure 3 for the three $CO_2$ mixtures and refers to calculations with the thermodynamic integration model coupled with the PC-SAFT EoS.
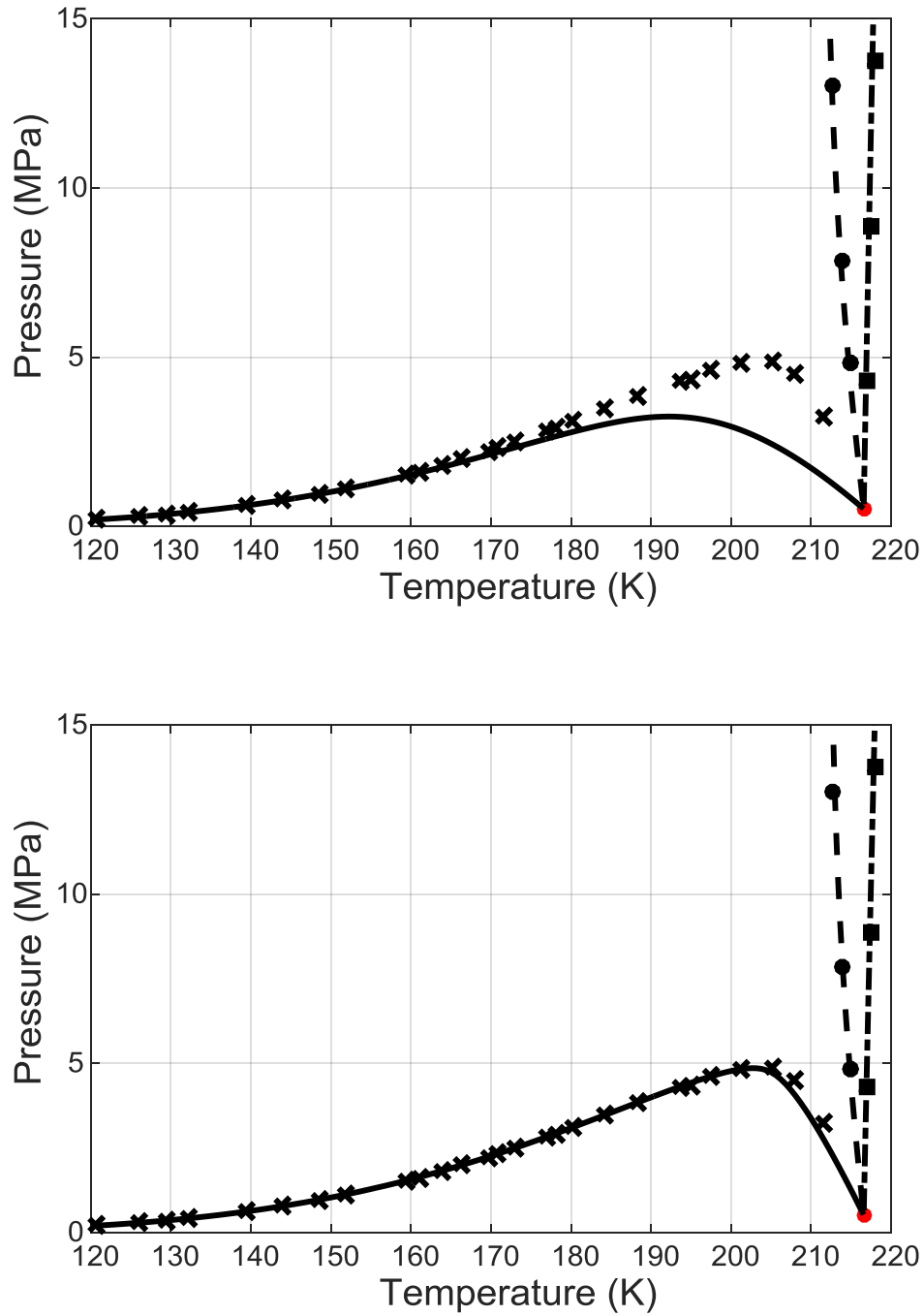
**Figure 3**. Calculation of the SLG equilibrium curves of binary $CO_2$ mixtures with the Thermodynamic Integration model, coupled with PC-SAFT EoS. Experimental data are represented by points for the following mixtures: (●) $CO_2 - N_2$, (■) $CO_2 - H_2$ and (**x**) $CO_2 - CH_4$. Calculations are shown with lines: (− − −) $CO_2 - N_2$, (− · −) $CO_2 - H_2$ and (−) $CO_2 - CH_4$. Top panel shows predictions ($\mathbf{k_{ij} = 0}$), while bottom panel shows calculations when temperature-independent $\mathbf{k_{ij}}$ parameters fitted to experimental binary VLE data are used.

### 3.3 Acquisition of Vapour Liquid Equilibrium Data for $CO_2$ Mixtures

Accurate knowledge of the thermodynamic properties of $CO_2$ mixtures is essential in the design and operation of CCS systems. The Vapour-Liquid-Equilibrium (VLE) of $CO_2$ mixtures is, for example, one of the basic parameters required to design a $CO_2$ capture process as well as non-condensable gas separation processes. Available experimental data and the theoretical models associated with the thermodynamic properties of $CO_2$ mixtures within the operation window of CCS are scarce (Ahmed et al., 2014). This is particularly the case for multi-component $CO_2$ mixtures. However, it should be noted that CCS processes cover a large range of operation conditions from atmospheric pressure to supercritical states, therefore experiments alone cannot satisfy the requirements of engineering applications (Chapoy et al., 2013). In order to exceed the limitations of the available experiments theoretical models in the form of EoS need to be developed using experimental data. However, many EoS available in the literature do not show any clear advantage in CCS applications for the calculation of properties of multi-component $CO_2$ mixtures. Hence, the objective of this work is to conduct experiments with $CO_2$ mixtures relevant to the CCS chain to obtain experimental data that can be used to develop reference equations of state for CCS applications.

CanmetENERGY is providing experimental VLE data for multi-component $CO_2$ mixtures to support our efforts to develop EoS relevant to CCS systems. In this context, CanmetENERGY has built a $CO_2$ pressure cell test facility capable of reaching and maintaining a two-phase equilibrium for multi-component $CO_2$ mixtures while separately measuring the composition and density of both liquid and vapour phases (Figure 4). Under this collaborative effort, experimental VLE composition and density data is acquired for three different $CO_2$ mixtures; namely $CO_2$-$O_2$-$N_2$-Ar, $CO_2$-$SO_2$-$N_2$, and $CO_2$-$CH_4$-$N_2$. This data is acquired in the ranges 300 to 220 K at increments of 20 K and 5 to 80 bar at increments of 5 bar. Experiments are performed in a thermally stable environment where the temperature is controlled to 0.01 K. In addition to tight temperature control, equilibrium of the two-phase mixtures is maintained by a pump that continually mixes the two-phase mixture to ensure that equilibrium is achieved and maintained throughout the experiments.
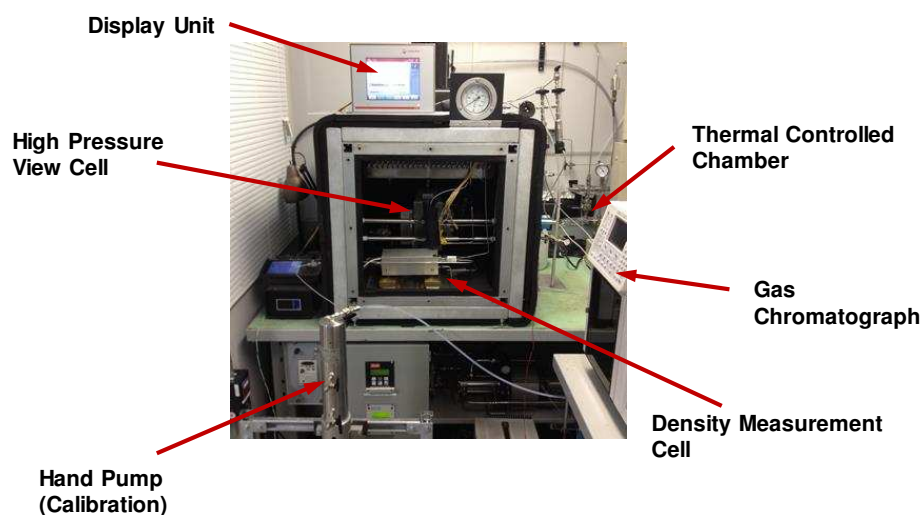
(a)
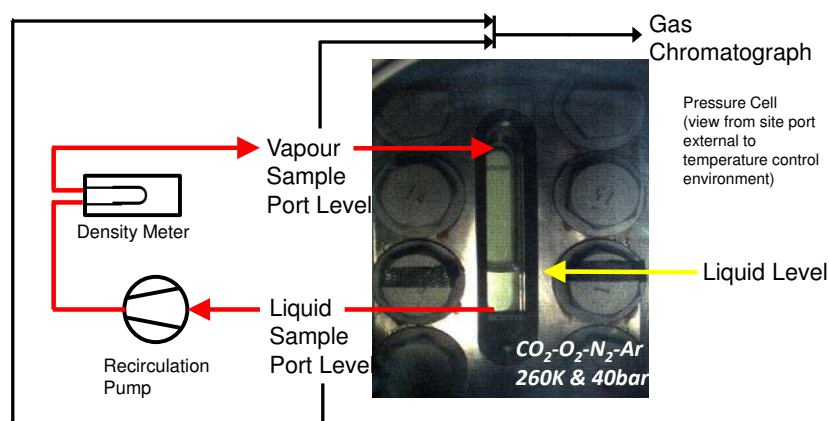


(b)

**Figure 3**. CanmetENERGY's $CO_2$ Pressure Cell Test Facility (a); and, sampling arrangement (b).

Main Research Outcomes

At the outset experiments were conducted with pure $CO_2$ to set the baseline and verify the methodology, calibration procedures, accuracy and consistency of the measuring devices. Data from the National Institute of Standards and Technology (NIST) (Chickos, 2005) was used as a control dataset. Subsequently tests were conducted with the selected quaternary $CO_2$ mixtures discussed above. The experimental data were compared with pure $CO_2$ measurement results, similarities in the general trends in the vapour phase were observed but more pronounced differences existed in the liquid phase. Further, quaternary $CO_2$ gas mixtures were prepared and tested within the targeted ranges of pressure and temperature,

VLE composition and density data was acquired and compared to HYSYS simulation results using the Peng–Robinson EoS (HYSYS, 2014; Peng and Robinson, 1970). There were some deviations from predicted HYSYS results at high pressures, particularly in the vapour phase, as depicted in Figure 5; however the overall trends showed reasonable agreement. The experimental data was shared with NCSR to further adjust and verify their equation of state. The outcome of the latter activity has been presented in the previous section.
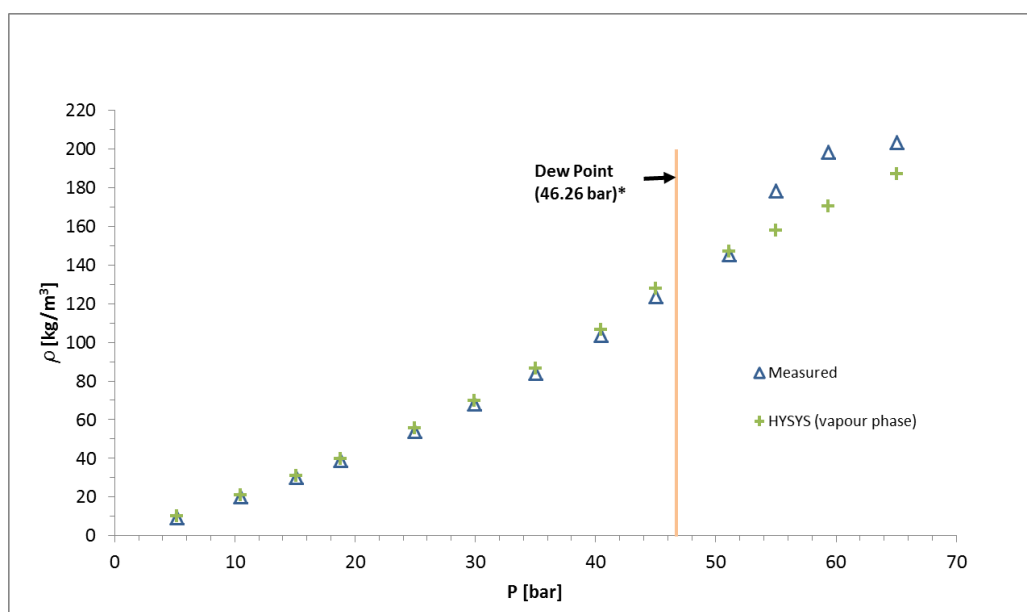


**Figure 5**. Vapour phase density measurement HYSYS (Peng-Robinson EOS) Calculated Value vs. Measure $CO_2$-$O_2$-$N_2$-Ar as Mixture (93%-5.41%-1.49%-649 ppm), T = 280K.

The experimental work conducted by CanmetENERGY led to a unique database for the properties of $CO_2$ mixtures that are relevant to CCS systems. Moreover, this experimental campaign provided the research team at CanmetENERGY with the opportunity to optimize and fine-tune their experimental apparatus, calibration, sampling and test procedures. In this respect extensive and unique operational experience was gained. This capacity can be made available to other research initiatives in order to support future EoS development or other research efforts.

# 4. WP2 – CO$_2$ Transport

## 4.1    Pressure drop and compressor requirement

In this section we present the modelling of non-isothermal steady-state flow carried out in order to calculate pressure drop (and hence compressor power requirements) in pipeline networks transporting CO$_2$ with typical stream impurities using the dedicated EoS developed under WP1 (see figure 1 and Section 3.2). Compression strategies for minimising compressor power requirements have been developed. We have also performed parametric studies using a developed flow model to identify the type and composition of stream impurities that have the most adverse impact on the CO$_2$ pipeline pressure drop, pipeline capacity, fluid phase and compressor power requirements.

Compressor Power Requirements

Minimising the pressure drop and avoiding two-phase flows within CO$_2$ pipeline networks is essential for reducing compressor power requirements. This is critically important given that the compression penalty for CO$_2$ capture from coal-fired power plants is estimated to be as high as 12% (Moore et al., 2011). In order to evaluate the impact of CO$_2$ impurities on compressor power requirements a thermodynamic analysis method is applied to CO$_2$ streams captured using oxy-fuel, pre-combustion and post-combustion capture technologies, stream compositions were derived from Table 2. The analysis is performed for several methods of compression previously recommended for pure CO$_2$, including the following options (Witkowski and Majkut, 2012):

- Option A: Centrifugal integrally – geared multistage compressors.
- Option B: Supersonic axial compressors.
- Option C: Compressors combined with liquefaction followed by pumping.

Figure 5 shows an example of the calculation of thermodynamic paths for multi-stage compression combined with intercooling relative to the phase envelopes for pure and impure CO$_2$ streams. Figure 6 shows the power consumption for each compression strategy (options A, B and C) for mixtures representing all capture technologies.
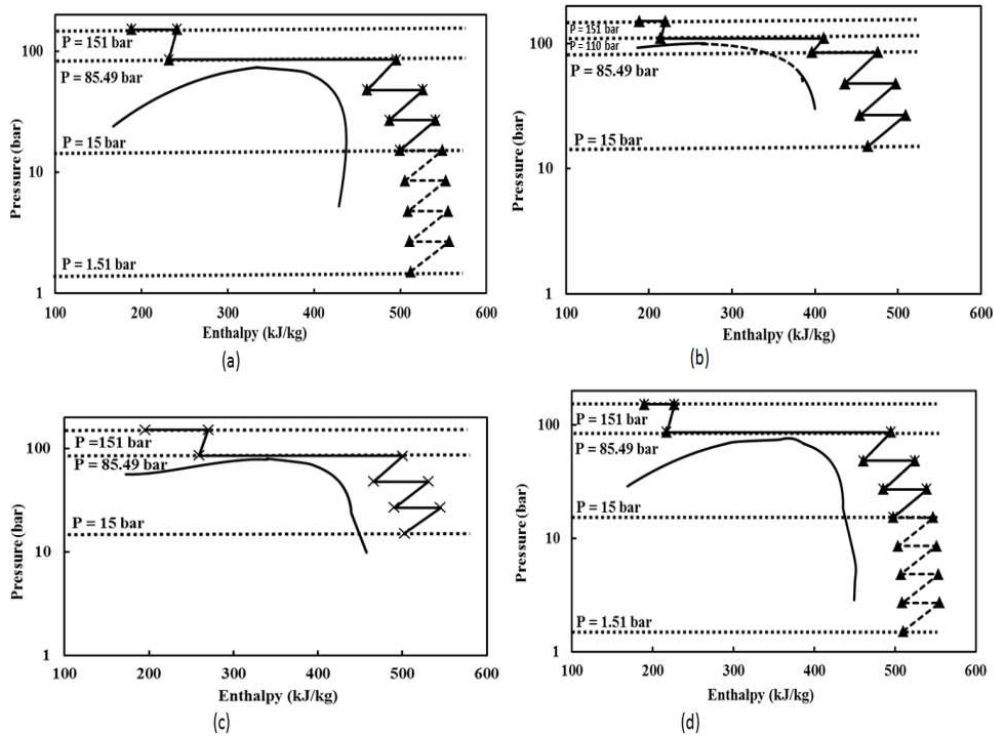
**Figure 5.** The thermodynamic paths for compression of pure $CO_2$ (a) and $CO_2$ mixtures from oxy-fuel (b), pre-combustion (c), and post-combustion (d) capture using compression and pumping with supercritical liquefaction. Note that the compressor inlet pressure is 1.5 bar for pure $CO_2$ and post-combustion streams and 15 bar for the pre-combustion and oxy-fuel streams.
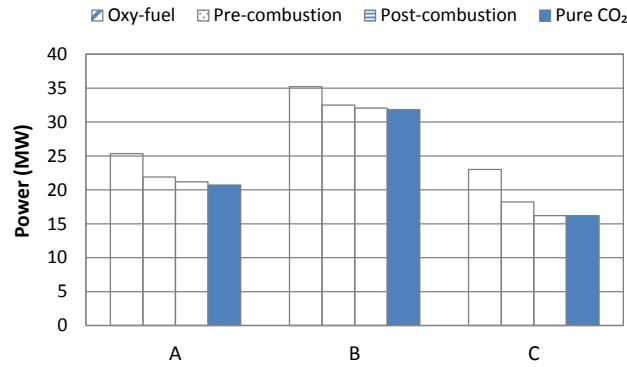


**Figure 6.** Power demand for multistage compression (options A, B and C) of pure $CO_2$, oxy-fuel (raw/dehumidified), pre- and post-combustion streams (compositions derived from Table 2).

## Non-isothermal Steady State Flow Modelling

To evaluate the impact of $CO_2$ impurities on pressure drop in pipelines a computational model was developed to resolve steady state flow in networks, including the ability to account for multiple input sources with varying flowrates, compositions and fluid properties.

This involves the solution of the following conservation equations for mass, momentum, energy and component:

$$\frac{d(\rho u)}{dx} = 0 \tag{1}$$

$$\frac{d\rho u^2}{dx} = -\frac{dp}{dx} - f\frac{\rho u^2}{2D} - \rho g \sin\theta \tag{2}$$

$$\frac{d\rho u\left(h + \frac{1}{2}u^2\right)}{dx} = \frac{4q_w}{D} - f\frac{\rho u^3}{2D} \tag{3}$$

$$\frac{dz_i}{dx} = 0, \ i = 1,\ldots,n. \tag{4}$$

where $x$, $D$, $\rho$ and $h$ are the local coordinate along the pipeline, the pipeline diameter, the density and enthalpy of the fluid respectively. u, P and $\theta$ respectively represent the velocity of flow, the fluid pressure and the angle of inclination of the pipeline with the horizontal axis. f and $q_w$ are the Darcy friction factor and the heat flux at the pipe wall, the calculation of which can be found in Martynov et al. (2015). The model has been applied to study the impact of variation in the feed flowrate from sources as well as the concentration of impurities upon the pressure and temperature profiles along the pipeline and the delivery composition for a given temperature of the feed streams.

Figure 7 (a) shows an example of the considered realistic pipeline network transporting $CO_2$ from Cottam and Drax power stations to the sequestration point at Morecambe South in the East Irish Sea. While Figure 7 (b) shows the pressure drop along this main truck line assuming a total feed flowrate of 25 Mt $y^{-1}$ as well as both an increase and decrease of 10 % from the Drax power station. In this case the $CO_2$ stream is a mixture of various impurities, including water, argon, nitrogen and oxygen, which are typically present in an oxy-fuel combustion $CO_2$ stream.

<table>
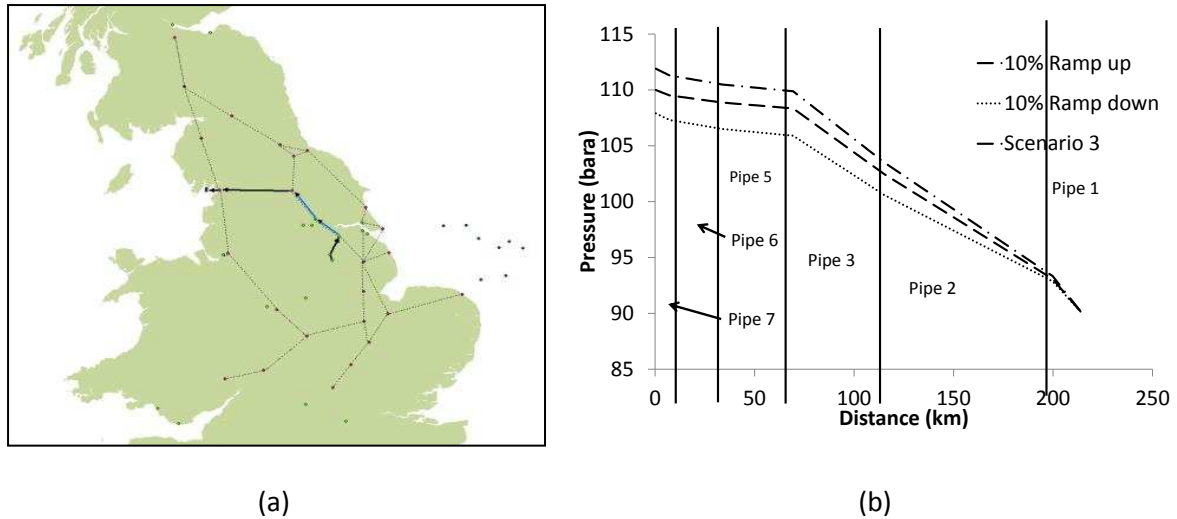<tr><td>(a)</td><td>(b)</td></tr>
</table>

**Figure 7.** (a) UK CCS pipeline transportation network, 2015-2025 (b) variation of fluid pressure along a main trunk pipeline for variations in the $CO_2$ flowrate from Drax power station (Brown et al. 2015).

As can be observed, in this case the alteration in the flowrate from just one of the $CO_2$ sources produces an increase in pressure drop of over 10 %. It has been found that variations in the feed composition can have a similar impact on the pressure drop even in this simplified case-study.

## 4.2    Small to medium scale pipeline releases

Medium-scale experiments involving high pressure releases of $CO_2$ containing a range of impurities from a pipe were performed at INERIS, France. The experimental rig and the measurement techniques were developed during the $CO_2$PipeHaz project ($CO_2$PipeHaz, 2009; Jamois et al., 2014). In $CO_2$QUEST, the same system was used to gain a better understanding of the influence of the presence of impurities on both the flow inside the pipe and on the external dispersion. The data were gathered for the validation of the mathematical models produced in $CO_2$QUEST.

The rig and equipment is shown in Figure 8. The pipe is 40 m long with a 50 mm internal diameter. Pressure (P), temperature (T) and heat flux transducers (F) were placed along its length at intervals of 10 meters. The pipe is thermally insulated. Calibrated orifices are placed at one end (6 mm or 12 mm - right hand side on Figure 8) while the $CO_2$ mixture is filled in

from the other end using a high pressure pump. The outflow near-field is also instrumented with pressure transducers and thermocouples (up to 50 cm from the orifice) to investigate the expansion zone. The measurement of the mass flow-rate is of great importance for the validation exercise of the models (Martynov et al., 2013). To do this, electronic measuring load cells were installed at six locations between the top of the supporting masts (in blue on Figure 8) and the bottom of the pipe. A transparent section is also installed in the middle section of the pipe to record video of the phase transition using a high speed camera. This also helps to check that the pipe is correctly filled. To produce "impure" $CO_2$ mixtures, the desired quantity of the chosen "impurity" ($N_2$ or $CH_4$ in this case) is injected in the pipe. The $CO_2$ filling is then completed to reach a pressure above the bubble point. The inventory is homogenously mixed by re-circulating the fluid through an external loop before experiments are carried out.
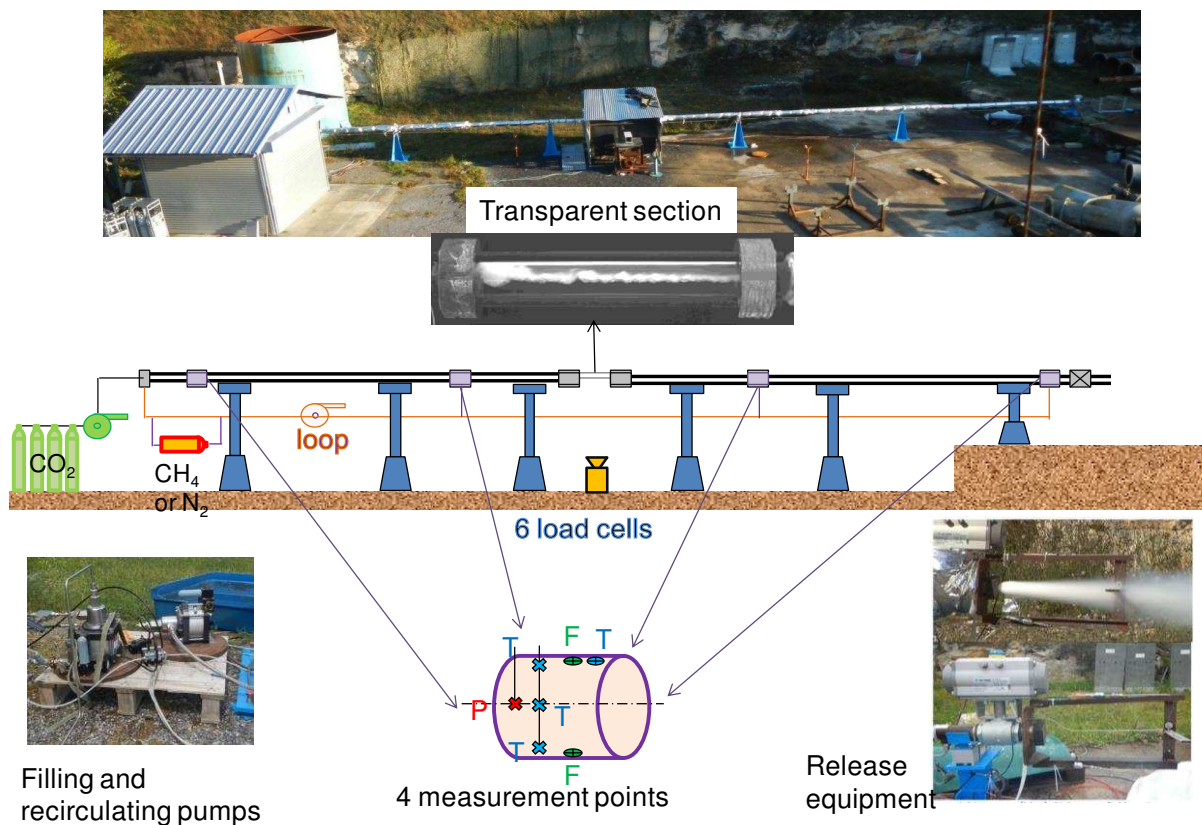


**Figure 8.** Presentation of the experimental rig constructed and operated by INERIS for "medium scale" $CO_2$ releases.

Twenty nine release experiments were performed varying the temperature and composition of the fluid and the diameter of the release orifice. Two experiments are discussed here to illustrate the experiments performed (Table 3): a 6 mm diameter release of pure $CO_2$ and a 12 mm diameter release with a $CO_2+N_2+CH_4$ mixture.

**Table 3.** Initial conditions of selected experiments.

| Test n° | | 1 | 2 |
|---|---|---|---|
| Mixture | | Pure $CO_2$ | $CO_2+2\%N_2+2\%CH_4$ |
| Pressure | [Bar] | 56 | 58 |
| Ambient temperature | [°C] | 17 | 10 |
| Orifice diameter | [mm] | 6 | 12 |

The mass flow rate is calculated using a temporal derivation of the measured mass (Figures 9 and 11).
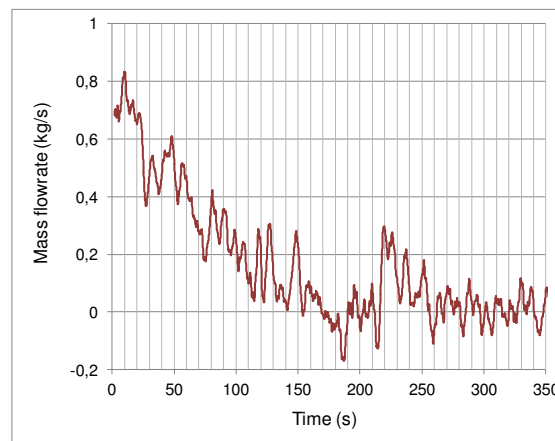


**Figure 9.** Mass flow rate (test 1:6 mm diameter, pure $CO_2$ release)
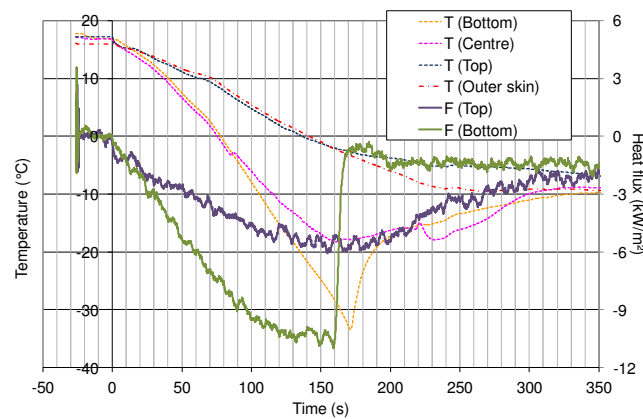


**Figure 10.** Temperature and heat flux measurements near the orifice during a 6mm diameter release (test 1: 6 mm diameter, pure $CO_2$ release)
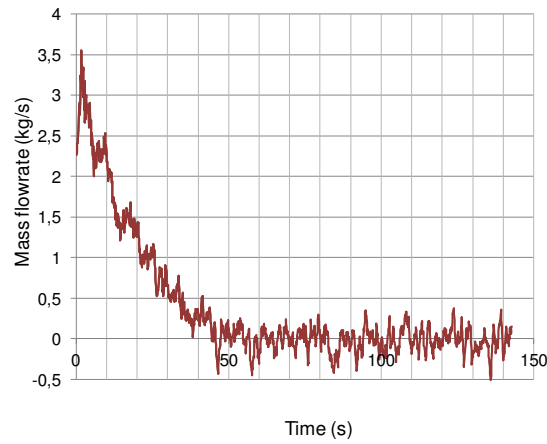
**Figure 11.** Mass flow rate (test 2: 12 mm diameter, $CO_2+2\%N_2+2\%CH_4$ mixture)
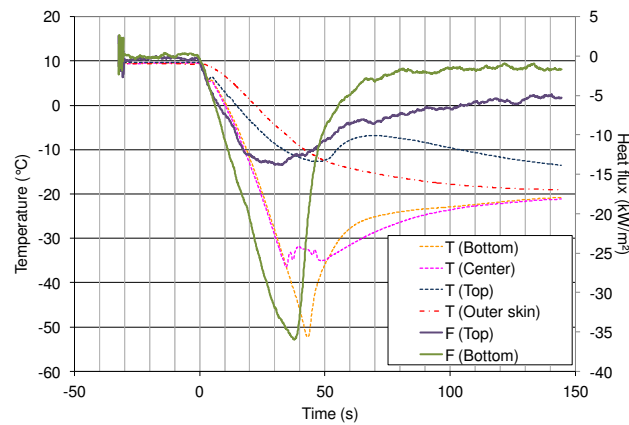


**Figure 12.** Temperature and heat flux measurements near the orifice during a 6mm diameter release (test 2: 12 mm diameter, $CO_2+2\%N_2+2\%CH_4$ mixture).

In both tests, during the first few hundred milliseconds of the release the fluid is nucleating but still seems homogenous. During the next period (until 23 s after the start of the release for test 1 and 4 s for test 2) a segregated two-phase mixture is present in the pipe but the level of liquid is above the orifice. The level of liquid reaches the orifice height 50 s after test initiation for test 1 and 12 s for test 2. After this the outflow becomes a gaseous jet. In the pipe the liquid disappears after less than 2 minutes for test 1 and approximately 35 s for test 2.

Further, modelling work often assumed pipe flow was adiabatic. An example of the evolution of the heat fluxes close to the orifice is shown in Figures 10 and 12. The various phases discussed above can be identified (liquid, two phase, gas). At the bubble point the heat flux

decreases abruptly while the temperatures remain almost constant suggesting a phase transition. This occurs earlier on the heat flux meters located on the top of the pipe where bubbles are forming. Subsequently the heat flux slope decreases in the gaseous phase (top of the pipe) while the slope remains much larger at the bottom, until the liquid is completely vaporized. This is certainly due to the vaporization of the liquid which absorbs energy from the metal of the pipe more rapidly than the vapour does due to its higher heat transfer coefficient. When the liquid is almost completely vaporized the thermodynamic conditions are close to the triple point and the heat flux measured at the bottom of the pipe decreases very abruptly and stays at a very low value until the end of the release, indicating no further vaporization is taking place. Contrariwise, the heat flux measured at the top of the pipe reverts to zero more slowly. This may be due to the conductive exchanges between the top and the bottom of the pipe through the thickness of the wall.

## 4.3    Large scale pipeline releases

The main objective of this section of the project was to conduct controlled large-scale experiments involving high pressure releases of $CO_2$ with a range of impurities. Experimental data recorded included near-field measurements of the dispersing jets and temperature measurements in the vicinity of a pre-designed crack geometry. This activity has provided experimental data that can be used to validate the CFD models developed as part of the project and described in the next section.

A fully instrumented industrial scale $CO_2$ pipeline was designed and built by Dalian University of Technology (DUT), China. The pipeline consisted of a main section with a length of 257 m and an internal diameter of 233 mm, a dual-disc blasting pipe with a length of 1 m, $CO_2$ injecting lines, a heating system (48 kW), a recoil force defender, a group of video recording systems and two data acquisition systems. Pressure and temperature data was recorded along the pipeline and in the dispersion area. Schematics of the pipeline are shown in Figure 13.
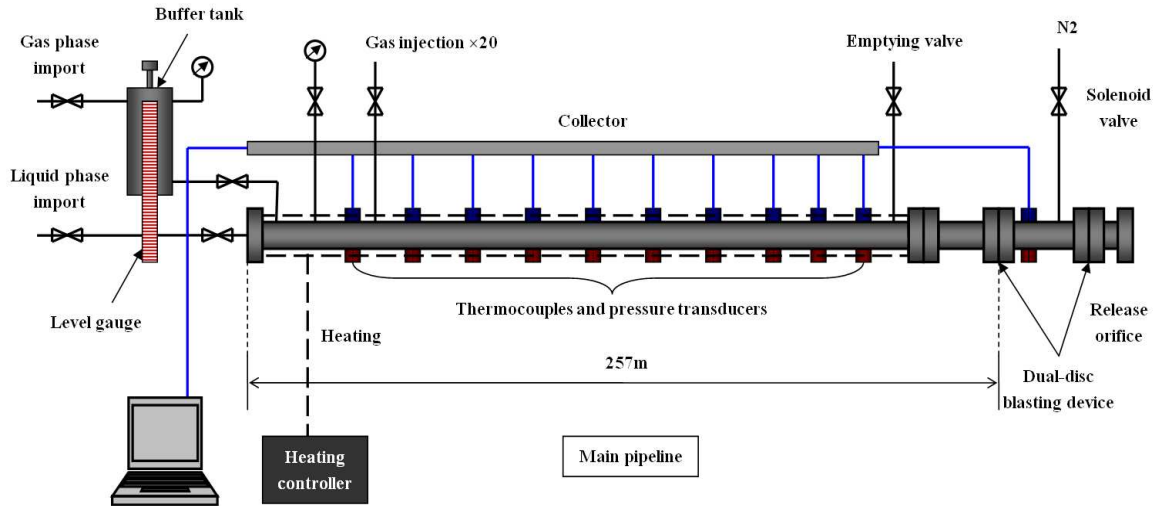
(a) Schematic diagram of the pipeline
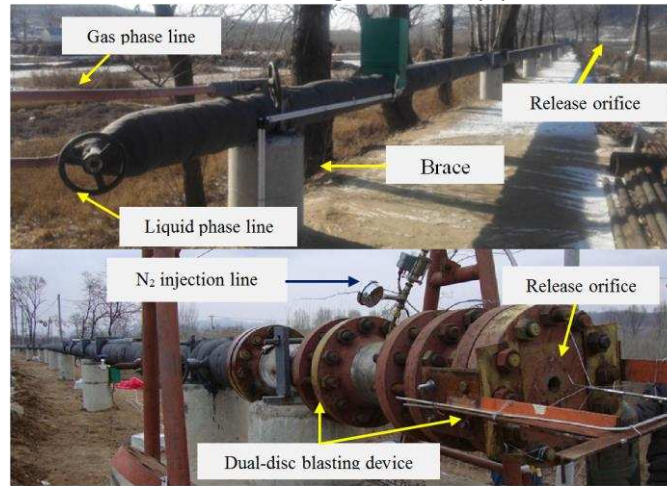


(b) Photograph

**Figure 13.** Schematic and real images of experimental apparatus.

Along the main pipeline, many pressure sensors and thermocouples were installed to monitor the pressure and temperature of the main pipeline and inventory during experiments. A large number of thermocouples and $CO_2$ concentration sensors were also arranged on vertical masts in the dispersion area at various distances from the orifice. Ten groups of $CO_2$ pipeline release experiments were performed with a range of impurities, initial inventory conditions and three discharge diameters including 50 mm, 100 mm and 233 mm (FBR). During release experiments the transient variation in fluid properties was recorded both in the pipeline and in the dispersion cloud. Additionally video recordings of the dispersing cloud were made from various locations, including from an overhead drone.

## 4.4 Near-field structure of, and heat transfer from, $CO_2$ releases

A computational fluid dynamic code developed under the EU FP7 project $CO_2$PipeHaz (http://www.co2pipehaz.eu/), capable of modelling the near-field structure and dispersion characteristics of releases of $CO_2$, has been extended to cover $CO_2$ mixtures with impurities and trace elements typical of those found in CCS streams. This includes both a continuous phase fluid model and a discrete-phase model capable of representing the distribution and properties of solid and liquid particles in such releases. The latter is an important consideration given the unusual phase behaviour of $CO_2$, and its sublimation from solid form at atmospheric conditions. The original model was based on solutions of the ensemble-averaged, density-weighted forms of the transport equations for mass, momentum and total energy. Closure of this equation set is achieved via the k-ε and Reynolds stress turbulence models corrected to accommodate the effects of compressibility. The use of a second-order accurate numerical solution scheme makes it possible to capture the detailed structure of the shock fronts that arise in accidental releases by using fine computational grids in the areas of interest. The computational cost of capturing such structures is reduced through the use of an adaptive mesh refinement (AMR) algorithm. AMR techniques have the advantage over uniform grids in physical space in that refined numerical solution meshes are only used at those points in a flow where significant change is taking place. Solutions are also calculated on each grid with a time step appropriate to that grid, with the whole refinement process controlled by using solutions to obtain an estimate of the truncation error. This approach is highly efficient since calculations in both time and space are performed only as required by the dictates of local numerical accuracy. Integration of the equations employs a second-order accurate finite-volume scheme in which the transport equations are discretised following a conservative control-volume approach. Approximation of the diffusion and source terms is undertaken using central differencing, and a Harten, Lax, van Leer second-order accurate variant of Godunov's method applied with respect to the convective and pressure fluxes. The complete model has been validated, e.g. Woolley et al. (2013), against experimental data obtained in a number of release scenarios including data on free jet releases and releases representative of punctures and ruptures of buried high pressure pipelines. It has also been demonstrated as part of an integrated, multi-scale modelling approach for the simulation of multi-phase dispersion from accidental $CO_2$ pipeline releases in realistic terrain (Woolley et al., 2014).

The model described above contains a composite equation of state (Wareing at al., 2013) for predicting the thermodynamic physical properties of carbon dioxide above and below the triple point, in all three phases (solid, liquid and gas) and at all phase changes, including the latent heat of fusion. In the present project the overall model is being extended to permit the dispersion characteristics of $CO_2$ and its impurities to be handled through the consideration of multiple scalars, with the effect of impurities on the thermodynamic physical properties accommodated using the equation of state developed by NCSR and that embodied in the TREND software package of Span et al. (2015). These provide relevant phase equilibrium and thermophysical data covering the range of impurities, operating pressures and temperatures applicable to the entire CCS chain. The presence of even small amounts of impurities can have a significant effect on the phase behaviour of $CO_2$ mixtures and must be considered as they account for changes in critical pressures and temperatures. The overall model is being validated against experimental data generated at different scales by project partners INERIS and DUT to demonstrate its usefulness for risk assessment purposes. Example predictions of the impact of impurities on near-field predictions of pure and impure releases are shown in Figure 14.
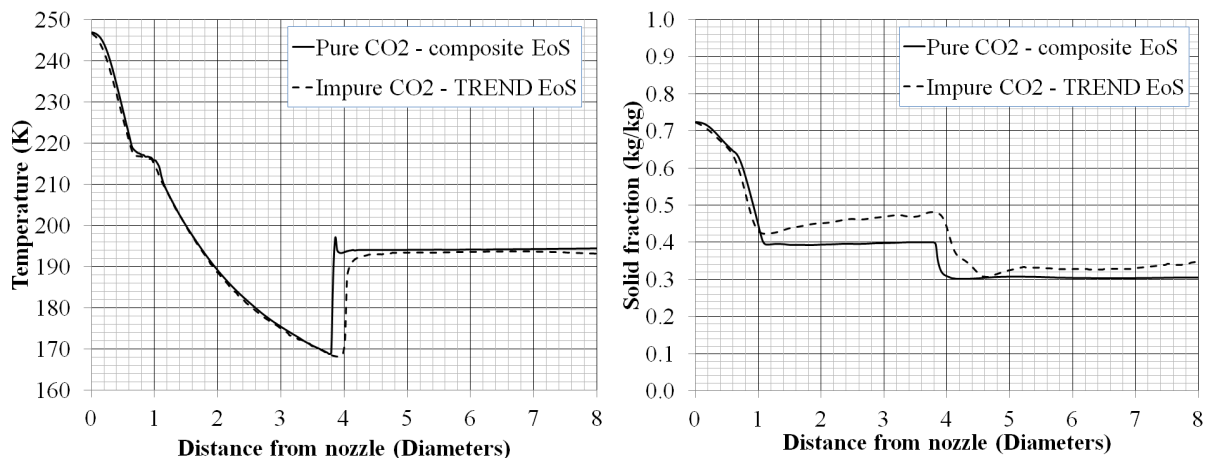


**Figure 14.** Shown are pure (100% $CO_2$) and impure (96% $CO_2$, 4% $N_2$) predictions of temperature (left) and solid fraction (right) in a near-field dispersion calculation, using a composite equation of state for the pure calculation (Wareing et al., 2013) and TREND 2.0 with solid $CO_2$ modifications for the impure calculations.

Further development of the model has also been undertaken to extend its capabilities to predict the heat transfer characteristics observed between a dense liquid release of $CO_2$

expanding through a puncture in a pipe and the pipe walls. Such an ability allows the prediction of crack-tip temperatures and pressures which can then be incorporated into crack propagation models, considered elsewhere in the project, to predict the propensity for a particular release scenario to escalate into a catastrophic incident due to running brittle fracture. It has been shown (Mahgerefteh and Brown, 2011) that changes in pipeline temperature by as little as 10° C can result in the transformation of a short crack into a fast-running long fracture, and it is anticipated that Joule-Thomson cooling will be affected by the presence of impurities in a release. The model described above was coupled to an appropriate transport equation for heat transfer in the solid pipe, using the thermophysical properties of typical pipeline steel, with the predictions of the complete model compared with data gathered by INERIS. Figure 15 shows the experimental set-up and associated computational details, together with model predictions of the velocity field outside the pipe. Table 4 demonstrates reasonable agreement with experimental temperature data at different times during a release of pure $CO_2$ at 277 K and 5.30 MPa for two of the thermocouple locations indicated in Figure 15(a). Similar levels of agreement were found at other measurement stations and in other tests.
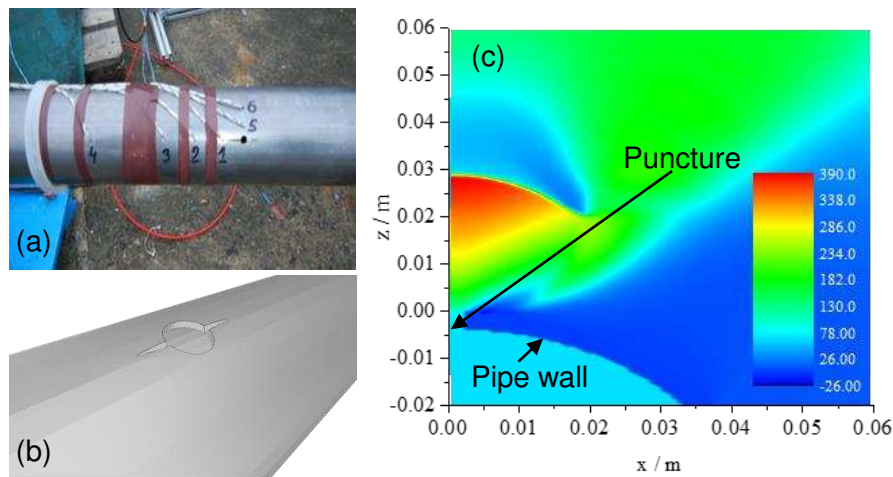


**Figure 15.** (a) Experimental rig showing thermocouple locations, (b) three-dimensional representation of the puncture and associated cracks, and (c) total velocity predictions at the puncture exit (in m s$^{-1}$).

**Table 4.** Comparison of experimentally observed and predicted pipe surface temperatures at three times during a release.

| Time / s | Temperature / K | | | |
| --- | --- | --- | --- | --- |
| | Thermocouple 2 | | Thermocouple 3 | |
| | Measured | Predicted | Measured | Predicted |
| 1 | 267 | 274 | 274 | 274 |
| 125 | 269 | 264 | 271 | 264 |
| 250 | 258 | 256 | 259 | 256 |

## 4.5 Brittle and ductile fracture tests and associated modelling

**Material Selection**

Different experiments were performed in order to compare the behaviour of three different steel grades that can be used for $CO_2$ pipelines. Steel grades X65, X70 and X80 have been compared under dynamic loading conditions. Firstly, Charpy V-Notch (CVN) and Drop Weight Tear Test (DWTT) experiments were carried out to monitor Ductile to Brittle Transition Temperature (DBTT) curves at different temperatures ranging from 20°C to -80°C. Based on performed dynamic fracture experiments it has been found that the X70 steel offers the best combination of strength, low temperature toughness and resistance to (accidental) $H_2S$ exposure as depicted in Figure 16.
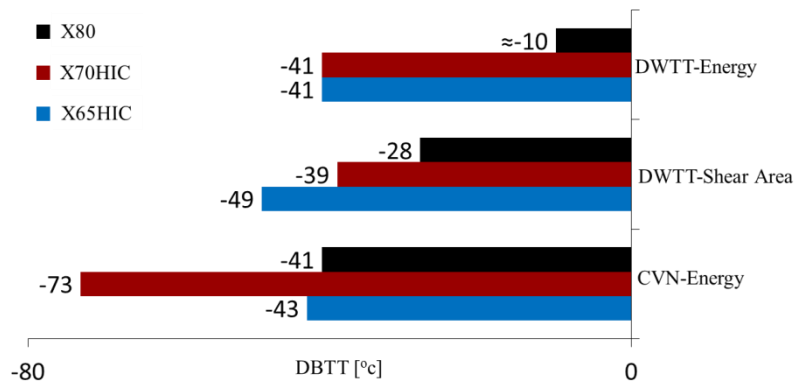


**Figure 16.** Comparison of DBTT between three steel grades X65, X70 and X80 according to CVN and DWTT.

**Ductile model**

The present study develops a fluid-structure coupling methodology for simulation of scenarios of pipeline failure involving ductile and brittle fracture propagation. To simulate the state of the fluid in the rupturing pipeline a one-dimensional compressible CFD model is applied. The proposed methodology couples the CFD model describing the pipeline decompression (Mahgerefeh et al., 2006; Brown et al., 2015) and the Modified Bai-Wierzbicki (MBW) material damage model (Döbereiner and Thibaux. 2013; Talemi et al., 2016a), which has been implemented in the Finite Element Analysis (FEA) code ABAQUS. The coupled fluid-structure ductile fracture model has been validated against experimental data reported in the literature on fracture propagation in a large-scale X70 pipeline (Makino et al., 2004).The developed coupled fluid-structure model was applied to simulate a full-scale burst test, showing that the coupled approach is capable of predicting the real fracture behaviour of pipeline steels under different dynamic loading conditions relevant to running fractures in real-scale high-pressure pipelines.

Figure 17 (a) shows the variation of the crack velocity with the crack length as predicted using the coupled fluid-structure fracture model (MBW+CFD) employing various numbers of cells in the CFD code with predictions using the HLP model and the experimental data. Figures 17 (b) and (c) show a photograph of a fractured pipeline taken from (Makino et al., 2004) and predicted corrugated deformation using the coupled fluid-structure fracture model, respectively.
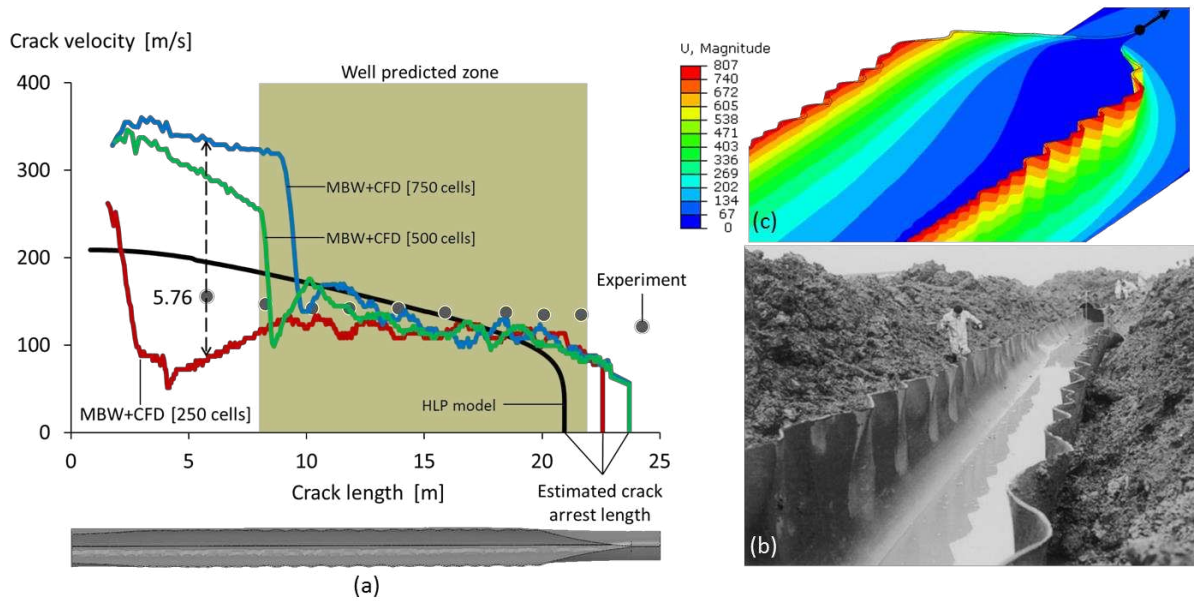
**Figure 17.** (a) Predicted crack propagation velocity by the MBW+CFD model and the HLP model in comparison with prolonged release experimental observations, (b) Photograph of a fractured pipeline taken from (Makino et al., 2004) and (c) predicted corrugated deformation using the coupled fluid-structure fracture model.

In terms of the brittle fracture model, a novel approach of the eXtended Finite Element Method (XFEM)-based cohesive segment technique has been used to model dynamic brittle fracture behaviour of pipeline steel (Talemi et al., 2016b). In this model the dynamic stress intensity factor and crack velocity are calculated at the crack tip at each step of crack propagation. To calibrate the brittle fracture model data from lab-scale experiments i.e. CVN and DWTT of X70 pipeline steel at low temperatures has been applied (Talemi, 2016). Using the methodology developed i.e. a hybrid fluid-structure modelling approach, a study is performed to evaluate the impact of $CO_2$ fluid phase and pipeline transportation conditions on the rate of brittle fracture propagation in a real-scale 48" OD pipeline. The model allows the quantitative prediction of the pipeline tendency to long running fractures in the form of the variation of crack length with crack velocity.

# 5. WP3 – EFFECTS OF IMPURITY GASES IN THE $CO_2$ STREAM ON ITS GEOLOGICAL STORAGE

The effect of impurity gases on the geological storage of $CO_2$ is studied in the $CO_2$QUEST project by a suite of methods ranging from laboratory and field experiments to predictive modelling and related model development. Two major field experiments are being carried out. In the first, supercritical $CO_2$ along with selected impurity gases is injected into a reservoir layer at a depth of 1600 m, the effects of such an injection on measurable quantities, such as pressure, temperature and in particular the chemical composition of the resident water will be investigated. Laboratory experiments are carried out on rocks from this site to investigate the effects of impurity gases on rock composition and to allow comparison between the laboratory and field results. In the second field experiment the focus is on scenarios mimicking potential $CO_2$ and impurity gas leakage into shallow aquifers. In this experiment industrial grade $CO_2$ is injected into a shallow water aquifer, followed by the monitoring of the injected fluid, its trace impurities and the potential mobilization of metallic trace elements from the surrounding rock. The modelling work has two main objectives; (i) to plan, predict and interpret the field experiments in order to gain understanding of the relevant processes happening in-situ and (ii) to make long-term predictions on the effect of impurity gases in large scale storage scenarios. In the following sections we will discuss some of the key aspects of the project and present some example results.

## 5.1    Deep $CO_2$ injection experiment at Heletz site, Israel

The Heletz site in Southern Israel has been developed for scientifically motivated $CO_2$ injection experiments with the objective of improving our understanding of the fate of geologically stored $CO_2$  in situ, in particular $CO_2$ spreading and trapping processes and developing methods for quantifying them from measurable quantities such as pressure, temperature and fluid samples. Extensive site characterization has been carried out and is summarized in Niemi et al (2016a; 2016b). The first of the planned $CO_2$ injection experiments are described in Fagerlund et al. (2013) and Rasmusson et al. (2014)) and will address in-situ measurement of residual and dissolution trapping of pure $CO_2$. These will be followed by experiments related to the effects of impurity gases in the injected $CO_2$ stream.

The site is located East of the city of Ashkelon (Israel) at the eastern edge of a depleted oil field. The target formation "the Heletz sands" comprises three sandstone layers "K", "W" and "A", having a cumulative thickness of ~10 meters. Above the reservoir, there is a caprock of ~ 40 m thickness mainly composed of shale and marl. The site was prepared as part of the EU-FP7 MUSTANG (coordinated by Uppsala University) and TRUST (coordinated by EWRE) projects. It comprises:

1. Two deep wells penetrating the reservoir to a depth of 1650 meters: well H18A, which is instrumented for $CO_2$ injection, fluid abstraction (via airlift), downhole pressure and temperature monitoring, downhole fluid sampling, Digital Temperature Sensing (DTS) via an optical fiber and chemical injection (for $CO_2$ saturation of water, tracer injection and impurities injection); well H18B, which is instrumented for fluid abstraction (via airlift), downhole pressure and temperature monitoring and DTS. The distance between the wells is 50 meters.

2. Three shallow wells (to a depth of ~250 meters): H18SA, H18SB and H18SC. These wells are intended for seismic monitoring of the injected $CO_2$ body.

3. A $CO_2$ injection kit (Figure 20): low flow (for $CO_2$ water saturation) and high flow (for $CO_2$ injection) pumps (Figure 19), a heat exchanger (Figure 18, for controlling the temperature of the injected $CO_2$) and a $CO_2$ storage tank. This kit is heavily monitored (P/T sensors long the path from the $CO_2$ tank to the wellhead) and is operated in semi-automatic mode.

4. A high pressure – high discharge air compressor for fluid abstraction via air-lift.

5. A high pressure nitrogen booster used for lifting fluid samples and purging of the injection system between injection sequences.

6. A control room to which all the monitoring technologies converge (including the seismic monitoring, measurements from the $CO_2$ tank, the wellhead and downhole measurements and the fluid samples). Facilities for onsite fluid characterization (including high pressure pH and EC measurement, mass spectrometer, alkalinity) are installed and integrated.

7. A line for the co-injection of $CO_2$-$SO_2$ and $CO_2$-$N_2$.

So far, the extensive characterization activities that have taken place include:

1. Geophysical logs conducted in both wells which have identified the target layers and the caprock.

2. Laboratory analysis of reservoir and caprock cores for mineral characterization, porosity/permeability measurement, hydro-mechanical characterization and chemical reactivity (carried out by CNRS-France, LIAG and Göttingen University

(Germany), Edinburgh University (Scotland). Impact of impurities at core scale has been investigated by CanmetENERGY of Canada.

3. Baseline Seismic survey, conducted by the Geophysical survey of Israel (GSI).
4. Hydrogeological characterization via pumping tests conducted in the wells. These show that the reservoir properties are rather favourable (permeabilities of ~720 mD).

The injection $CO_2$ system has been verified and successfully commissioned.



**Figure 18.** The heat exchanger.



**Figure 19.** Pump skid during commissioning.

**Figure 20.** Connection to the injection well.

## 5.2    Shallow CO$_2$ injection experiments at Catenoy site, France

INERIS conducted an injection experiment of industrial grade CO$_2$ into a shallow aquifer in order to simulate a vertical leak that is supposed to occur from deeper storage in a saline formation. A site for this experiment has been selected and equipped by INERIS in the chalky aquifer of the Paris Basin (France). Located at Catenoy (Oise), it contains 4 air-wells (wells dedicated to underground atmosphere measurement and sampling in the unsaturated zone) and ten piezometers (wells dedicated to water table measurement and groundwater sampling in the saturated zone), seven of which are represented on Figure 21. The well W2b was drilled in the frame of the CO$_2$QUEST project.
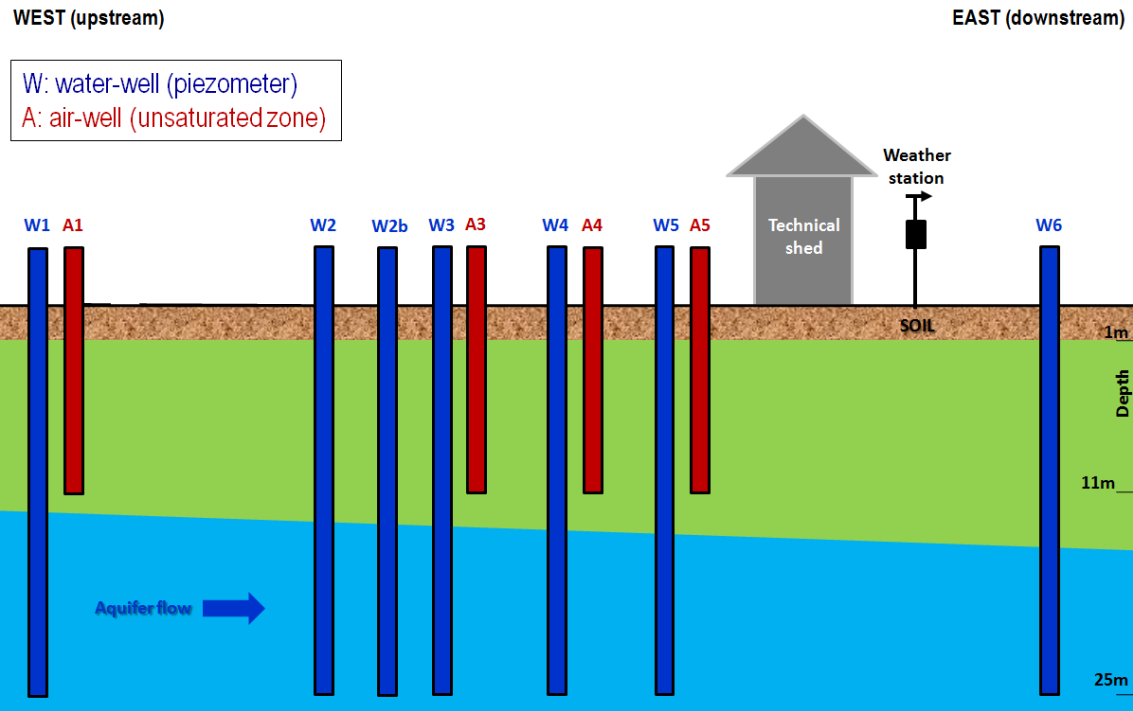
**Figure 21** Cross section of the experimental site of Catenoy (W2b is the new well drilled in the project).

This experiment was a "push-pull" test that began with a 3-hour "push phase" in which 3 $m^3$ of brine containing salt, dissolved $CO_2$ and impurities was injected, followed by the "pull" phase which consisted of pumping water back from the aquifer between 3 and 7 days after the push phase. This water was analysed and in situ monitoring was performed in the neighbouring wells, both in the water and in the gas phase above the water table.

A number of observations were made from this experiment:

- the injected plume was observed 5 m downstream during the "push phase"
- pH lowered by about 0.5
- the maximum concentration of dissolved $CO_2$ increased to 0.1 g/L
- the maximum concentration of certain metals increased to 0.5 mg/L for Zn, 0.2 mg/L for Li and 0.01 mg/L for As as shown on Figure 22.

Gaseous impurities were also observed in the unsaturated zone above the aquifer at the same time ($CO_2$ concentration increased to 600 ppm and He to 8 ppm). Additionally, during the pull phase more prolonged but less significant increases of some impurities were observed

e.g. dissolved $CO_2$ increased to 0.04 g/L and Li to 30 µg/L. It was also observed that He no longer degassed even when still present in the water and Zn concentrations remain below the detection limit.

There is an obvious buffer effect in the chalky aquifer due to calcite dissolution. By running simulations of the geochemistry with the PHREEQC code we concluded that experimental and modelled Zn concentrations were in very good agreement during the push phase (see the peak on Figure 22) but during the pull phase it was assumed that in situ measurements were under the detection limit while the model over predicts Zn concentrations at low levels. Compared with other studies conducted by INERIS and with others from the literature this suggests that adsorption of iron oxides plays a key role in the transport of Zn and other metallic impurities. Future models will have to take this effect into account.



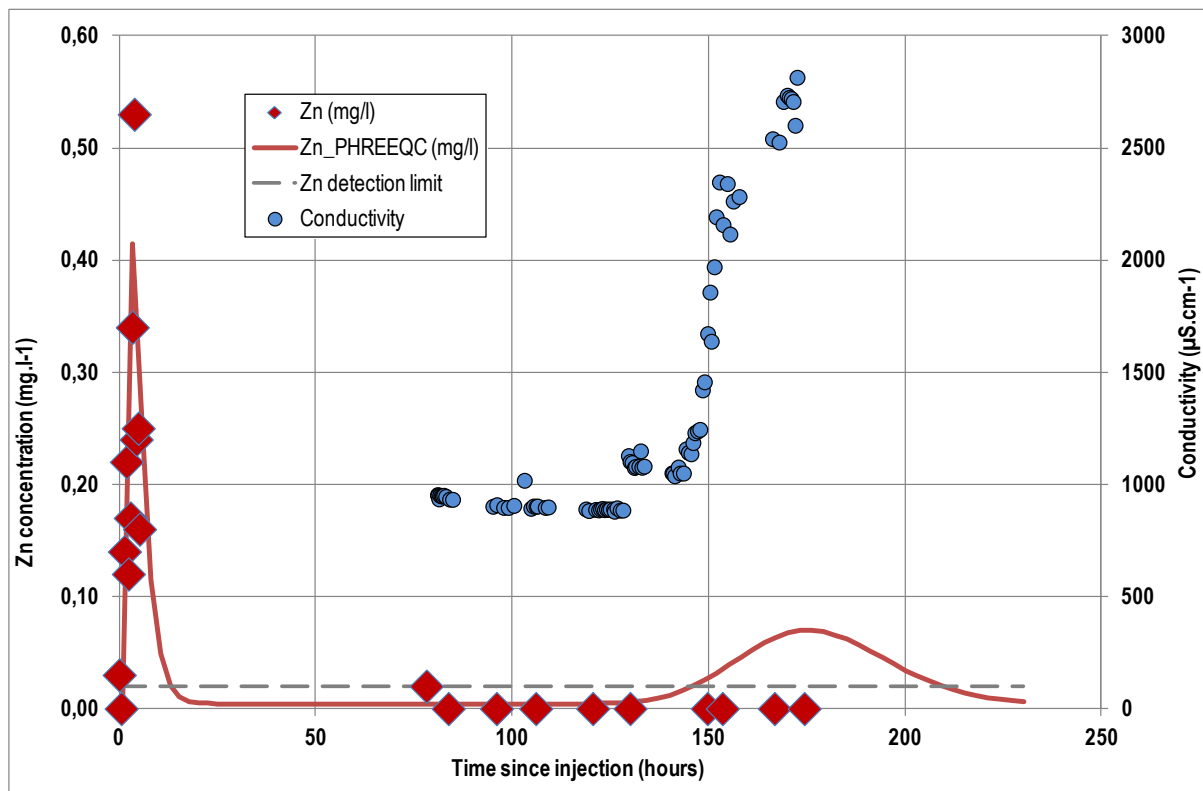**Figure 12.** Experimental and simulated concentrations for Zn at well W2b, located 5 m downstream of the injection well.

These results indicate that the impact in the aquifer is very limited both for $CO_2$ and the impurities injected. After several days the impact is not noticeable further than a few dozen of meters. However, this result depends on the conditions of this field experiment. In order to

simulate a leakage from a storage located in a deeper geological formation it would be useful to perform an injection test for a longer period.

## 5.3    Modelling of $CO_2$ and impurity gases spreading in geological formations

Based on the review of the characteristics of impurity gases in the $CO_2$ stream and their potential impact on geological storage, two impurity gases were selected for the field experiment at Heletz; $N_2$ as it is expected to have a hydro-mechanical impact on gas/supercritical $CO_2$ flow and $SO_2$ for its expected geochemical impact. In the following sections their predicted effects are discussed.

### 5.3.1    Modelling of the hydrodynamic processes affected by impurity gases

The hydro-mechanical modelling of the spreading of a $CO_2$-rich phase was based on the well-known TOUGH2 simulator (Pruess, 2004). TOUGH2/ECO2N code as such is capable of simulating multiphase flow migration and mass partitioning of $H_2O$ and $CO_2$ in both brine-rich and $CO_2$-rich phases (Pruess and Spycher, 2007). Solid salt precipitation is also considered, dissolution/precipitation is calculated using local equilibrium solubility. However, the effect of multiple gases in the gas/$CO_2$ rich phase is not accounted for. For the purpose of modelling the effect of impurity gases the EoS included in the code was updated here. In this we follow the approach of Fagerlund and Niemi (2007). We assume the $CO_2$ rich phase to be a mixture of $CO_2$ and the impurity gases of interest. The movement of the gas phase, which depends on phase properties like density and viscosity, is governed by the properties of the gas mixture. In our numerical implementation we allow the composition of this gas mixture to be continuously updated with time as the different gases of the mixture dissolve into brine at different rates according to their specific solubilities. With this approach we assume that the gas mixture consisting of $CO_2$ and impurities does not separate within the gas phase itself and can therefore be treated as a so-called pseudo gas mixture representing the fluid properties of the mixture as calculated from the updated EOS.

In practice this is implemented into the TOUGH2 code as follows: during the simulation, we first compute the mass fractions of the different gases in the gas mixture. We then calculate the gas properties of each component gas, for example, compressibility factor, fugacity, and solubility of each gas into the brine phase by using the thermodynamic equations developed

by Duan and Mao (2006) and Duan et al. (2007). We then calculate density, viscosity and enthalpy of the gas mixture. These physical properties are determined by the external program REFPROP developed by U.S. National Institute of Standards and Technology (NIST). This program uses Kunz and Wagner models for gas mixtures (Kunz et al., 2007). After advancing a time step dissolved mass in the brine will be subtracted from the initial gas contents and the mass of each gas is updated for the next time step.

**Hydro-mechanical impacts of $CO_2$ and $N_2$ co-injection**

The modified TOUGH2/ECO2N code was used to model the reference push-pull $CO_2$ injection experiment at Heletz (Rasmusson et al, 2014) and to predict what effect the $N_2$ gas would have on the experiment result. $N_2$ was chosen as the example impurity gas for these simulations as it can alter the density and viscosity of the $CO_2$ plume significantly, thereby giving an estimate on the physical influence of impurities on pressure and migration while not reacting chemically with the target formation. The experiment described by Rasmusson et al (2014) is simulated and the pressure response and plume migration of the pure $CO_2$ case is compared with that of gas mixtures with an $N_2$ content of 5 % to 10 %. The simulated test sequence with pure $CO_2$ is presented in Rasmusson et al. (2014). Here we simulate the early part of this test sequence both with and without $N_2$ in the $CO_2$ stream in order to estimate how the physical transport processes will be impacted. In this sequence we first inject pure $CO_2$ for the sake of reference and then co-inject $CO_2$ with a 5 % to 10 % mass fraction of $N_2$ to compare the respective hydro-geologic responses on key variables such as pore pressure evolution and plume migration.

The temporal variation of pore pressure during the simulated experimental sequence is shown in figure 23. In all cases pressure increases during water injection and decreases following mass production. The pore pressure rises again during the co-injection of $CO_2$ and $N_2$, then drops and stabilizes after injection. In general, a higher pressure is observed when a larger $N_2$ content is applied, with 10 % and 5 % of $N_2$ creating overpressures (in comparison to the pure $CO_2$ case) of about 450 kPa and 225 kPa, respectively. The density decrease of the gas mixture also impacts the plume migration. By increasing buoyancy the plume becomes lighter and moves further compared to the pure $CO_2$ case (figure 24). Mixing $N_2$ with $CO_2$ decreases the viscosity of the resulting gas mixture which eventually affects the mobility of the gas phase because the hydraulic conductivity is inversely proportional to the viscosity.

Solubility changes of each gas component in the brine phase were also investigated. After $CO_2$ and $N_2$ injection for 12 days, the $CO_2$ mass fraction in brine increases up to ca. 4.7 % in the case of pure $CO_2$ but only to about 4.5 % with an $N_2$ content of 10 %. $N_2$ solubility is directly proportional to initial content in the gas mixture and increases up to about 0.012 % when 10 % of $N_2$ is co-injected. The simulation results showed a linear correlation with initial mass ratios of gas mixture because the solubility of a gas component into brine is primarily controlled by the partial pressure of each gas in the gas mixture. Overall however, the hydrodynamic/hydro-mechanical effects are relatively small and we can expect greater impacts on geochemistry with different impurity gases, this will be discussed in the following section.



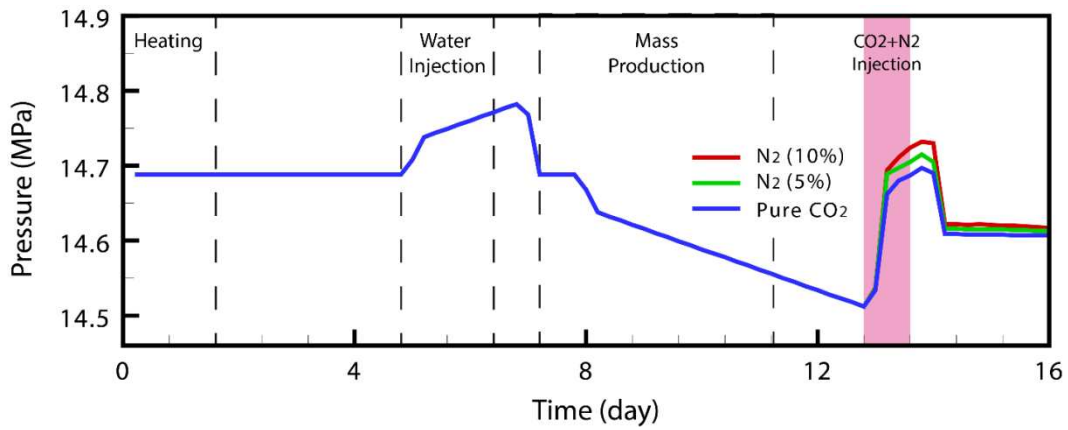**Figure 23**. Temporal variation of the pore pressure during the push-pull experiments with the schedule suggested in Table 2. In all cases, pressure increases during the water and $CO_2+N_2$ injection and it shows a higher increase when the concentration of the impurity is higher. Note that the red line represents the 10 % $N_2$ case, green the 5 % and blue the pure $CO_2$ case (Rebscher et al., 2014).
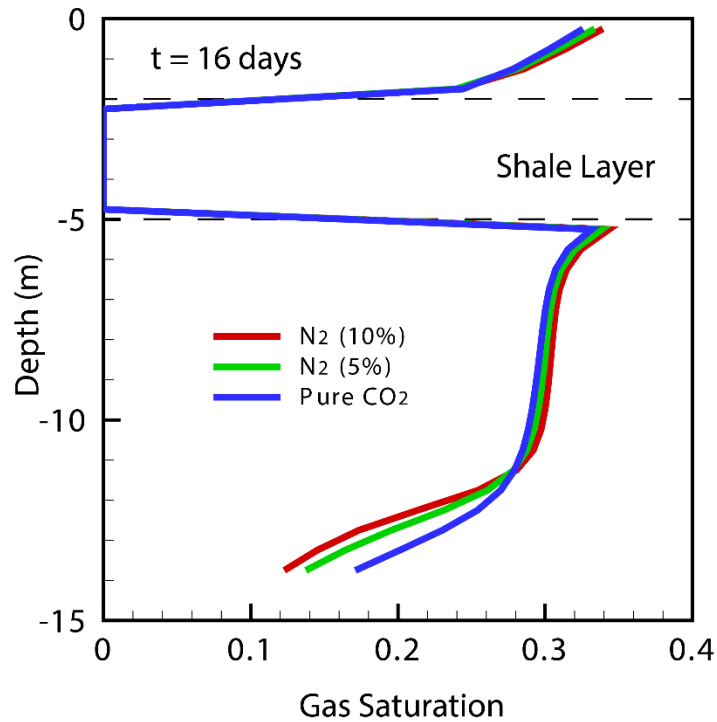
**Figure 24.** The depth profile of gas saturation at t = 16 days after the push-pull experiment. The plume shape from higher $N_2$ contents shows faster migration and move further upward because of density and viscosity decreases in the gas mixture (Rebscher et al., 2014).

**Model for the geochemical effects**

In addition to the impact of inert gases in a $CO_2$ stream it is of interest to analyse the effects of geochemically active impurities, both on the reservoir rock and on the caprock. Again Heletz data was used based on detailed mineralogical and petrophysical data provided by Edlmann et al. (2016) and Niemi et al. (2016) for the parameterisation of the generic models. These 1D and 2D radial models represent a sequence of the reservoir complex i.e. sandstone, shale, sandstone under a caprock, at reservoir scale. The 2D radial model covers a height of 16 m and a radial distance of 30 km, measured from the injection well. For the numerical simulations the coupled thermal, hydrological, chemical code TOUGHREACT V3.0-OMP from Lawrence Berkeley National Laboratory (Xu et al., 2014) was applied. This recent version features the special ability to implement transport of additional trace gases within the $CO_2$ rich phase. The study discussed in Wolf et al., (in prep.) is one of the first addressing $SO_2$ and $NO_2$ as a trace gas in the $CO_2$ stream, hence providing a significant contribution to understanding the impact on deep geological storage of impurities within a $CO_2$ stream.

The injection scenario discussed here consists of co-injecting $CO_2$ and $SO_2$ with a ratio of 99 % to 1 % at a constant rate of 9 kg/s over a period of 10 years. The numerical simulations demonstrate a preferential dissolution of $SO_2$ in the brine causing a strong reaction with the carbonate phases. Whereas the $SO_2$ is limited to the region of the bottom sandstone, $CO_2$ migrates through the intermediate shale layer and spreads in the upper sandstone along the contact with the caprock about a radial length of 80 m. Spatial differences of the impact of the two gases are obvious in the range of the lateral impact on the bottom sandstone. At the end of the injection period maximum horizontal distances of less than 200 m and about 2000 m were reached by $SO_2$ and $CO_2$ respectively in the case described.

Naturally changes in porosity are not only dependent on the fluid injected but also on the minerals present in the reservoir. In the Cretaceous sand layers at Heletz the initial porosity of the bottom sandstone layer is approximately 15 %. The dissolution of ankerite associated with the precipitation of anhydrite leads to a net porosity increase of about 0.5 %. Noteworthy is the self-sealing effect of the shale layer which is induced by the intrusion of $SO_2$ leading to a conversion of calcite to anhydrite. Here the decrease in porosity at the border between the lower sandstone and the intermediate shale layer amounts to a value of 1 %. But as the initial porosity of the shale layer was assumed to amount to less than 10 % this relates to a significant decrease in permeability. This stresses the importance of including chemical aspects while investigating thermal and hydrological processes and the necessity of site-specific evaluation, for further details see Wolf et al., (in prep.).


**Long-term effects**

Modelling of the laboratory and field experiments will enable model validation. Such validated models can be used with better confidence to make long-term and large-scale predictions. Even in the long term the processes of geochemical alteration and changes in two-phase flow properties discussed above will be important. An additional aspect is how impurity gases may influence dissolution and density driven convection, a process known to enhance solubility trapping. We investigate this effect for several co-contaminants ($N_2$, $CH_4$, and $H_2S$) by accounting for the impurity effects on both gas solubility and induced density changes driving the convective mixing. The study is conducted using multicomponent density-driven flow simulation with the USGS SUTRA-MS model which accounts for the relationship between a dissolved specie's mass fraction and the density change of the aqueous

phase, as well as the impact of dissolved $CO_2$ on the aqueous phase viscosity. Effects of impurities on the convective mixing are studied specifically in regard to the changes in onset time of convection, dissolution rate, flow pattern and solute distribution. The results show that the impurities investigated have the potential to reduce the convective mixing and the enhanced solubility trapping of $CO_2$. However, the effects on the convective mixing are limited due to the relatively small concentrations of impurities found in field.

# 6. WP4 – FULL CHAIN CCS TECHNO-ECONOMIC MODELLING

In this section we present a techno-economic analysis of gas purification and compression for $CO_2$ capture, shared capture infrastructure and $CO_2$ transport networks.

**$CO_2$ Compression and Purification Units**

Oxy-combustion capture is currently one of the most promising methods of $CO_2$ capture as it is one of the most developed and technologically mature methods for CCS. Unlike other mature technologies, oxy-combustion capture presents a trade-off between cost and purity. Oxy-combustion capture consists of an air separation unit (ASU) that produces a high purity oxygen stream and, mixed with recycled flue gas, provides a high-oxy environment in which to burn the fuel. The flue gas produced by oxy-fuel combustion will vary in purity depending on the input conditions and still requires dehydration, further purification and compression in order to be suitable for transport and storage. The latter is performed by means of a $CO_2$ Compression and Purification Unit ($CO_2CPU$).

In this work we have modelled four variations of the $CO_2CPU$ in Aspen HYSYS using a Peng-Robinson property method with each system varying in their method of separation. These models were based on similar models presented by Posch and Haider (2012). The four models in order of descending complexity are: a $CO_2CPU$ with a 6-stage distillation column, one with a double flash system with heat integration, one without heat integration and the least complex with only compression and dehydration. The results from these models show that an increase in product purity and complexity results in a reduction in capture efficiency. The capital and operational cost results for each $CO_2CPU$ modelled were translated into a price for the $CO_2$ product stream shown in figure 25. In order to derive a price for each product it was assumed that the $CO_2CPU$ is an independent entity in which to invest, with

two inlet streams - raw flue gas (free) and energy (cost) - and two outlet streams - $CO_2$ product (revenue) and waste stream. Figure 25 shows that at four different minimum rates of return (equated to the internal rate of return IRR) we find a non-linear and non-monotonic relationship between $CO_2$ price and purity. The difference between the highest purity product at 99.98 wt.% CO2 and the lowest purity product at 82.91 wt.% CO2 represents a 42% reduction in price.
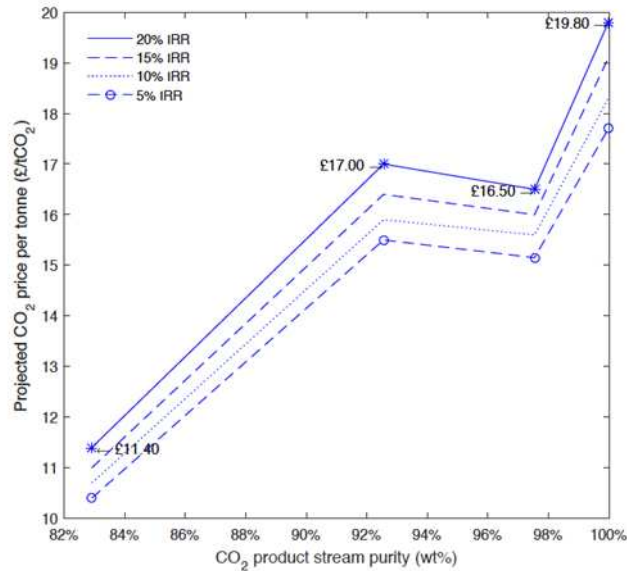


**Figure 25.** Graph showing the $CO_2$ price per tonne sold if marketed assuming a minimum rate of return on investment of 20%, 15%, 10% and 5% on the $CO_2$CPU as a function of $CO_2$ stream purity.

## $CO_2$ Compression and Purification Units

Certain considerations must be taken into account however in terms of the product purity. A large presence of non-condensable gases can reduce storage capacity and also requires larger pipeline diameters for an equivalent amount of pure $CO_2$ at a given pressure. Typically it is recommended to have a purity level for $CO_2$ of 96% (de Visser et al., 2008). Nevertheless, if a combination of cheaper, low purity sources of $CO_2$ were mixed with higher purity sources of $CO_2$ in a transport network a final trunk line with a $CO_2$ stream composition suitable for injection could be achieved. In order to describe this kind of system we have taken a UK based case study with 10 gas CCGT plants, 10 coal fired plants and one steel industrial plant set up by Prada et al. (2011). Each CCGT plant was assumed to adopt amine-based post combustion capture while the coal plant and steel plant adopt oxy-combustion capture,

choosing from one of the oxy-combustion $CO_2CPU$ models described. This scenario was formulated into a bi-objective optimization problem in GAMS, looking at the trade-offs between optimizing for lowest cost and highest purity. Binary variables of values 0 and 1 were used to represent the choice of $CO_2CPU$. Figure 26 shows the Pareto front for the competing objective functions: minimum cost and maximum purity assuming a lower bound for $CO_2$ purity at the trunk line of 96 wt.%. The results in figure 26 show the average capital and operational costs per tonne of $CO_2$ captured for the $CO_2CPU$ applied to both post combustion and oxy-combustion capture. The difference between the capital cost for a minimum purity system and the maximum purity system per tonne of $CO_2$ capture is 45%. Applying the same assumptions as earlier for the $CO_2$ price, this difference represents a 17% increase in $CO_2$ price.

**Shared Capture Plant Infrastructure**

With the objective of further reducing the costs of oxy-combustion capture we have studied the financial benefits of having a shared $CO_2$ compression and purification unit with a throughput of 20 Mt $CO_2$/year (equivalent to the output of a large power plant such as Drax) as opposed to having four $CO_2CPUs$ each with a throughput of 5Mt/year.
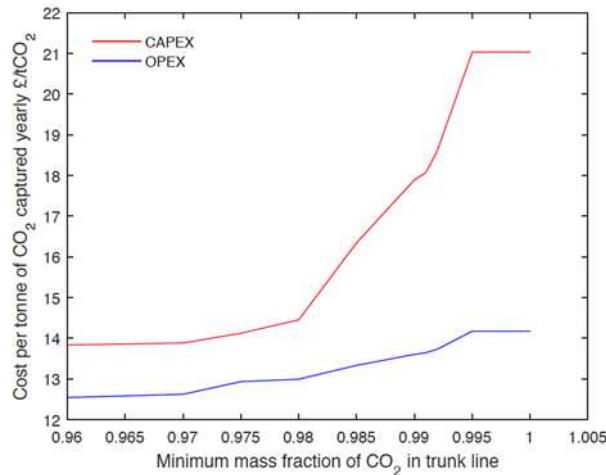


**Figure 26.** Graph showing the network capture system CAPEX and OPEX per tonne of $CO_2$ captured yearly as a function of minimum trunk line purity – optimization problem Pareto front.

In this study we do not include transport costs, however these are deemed to be significantly lower than capture costs: onshore pipelines are 25-30 times less cost intensive per tonne of $CO_2$ than the cost of capturing (Prada et al., 2011). The results of this study show that having one large 20Mt $CO_2$/year plant reduces the total capital expenditure by 16% and the yearly operating expenses by 4% compared to having four 5Mt $CO_2$/year units. Hence, we can conclude that adopting shared $CO_2$ capture infrastructure helps reduce the investment risk of CCS.

# 7. WP5 – CO$_2$ IMPURITY IMPACTS AND RISK ANALAYSIS

To fulfil the objectives of the CO$_2$QUEST global assessment, INERIS proposed a tool to estimate the different effects (or impacts) of various impurities in a $CO_2$ stream along the entire CCS chain. After a review of risk analyses for CCS performed by INERIS or by other authors[1] - completed by the expertise of CO$_2$QUEST partners, we identified and divided all relevant effects for impurities into three categories. i) Physical effects which have consequences on the CCS chain (e.g. reduced capacity or increased costs) without preventing its "normal" function, contrary to the other two categories that refer to $CO_2$ leakage, therefore an "altered" function: ii) Chemical effects may increase the probability of leakage (e.g. by pipe corrosion or by degradation of well cement). iii) Toxic/ecotoxic effects may increase the severity of any consequences arising from such a leak (e.g. if an aquifer is contaminated). Table 5 gives an overview of the 6 indicators that were finally selected (column 2). It may be observed that $CO_2$ stream density has an effect on transportation and storage.

---

[1] Mainly Farret et al., 2011ª, 2011b; Birkholtzer et al., 2009; Condor et al., 2010; Oldenburg, 2006; Savage et al., 2004; Dodds et al., 2011, Wilday et al., 2011, Mohitpour et al., 2011. Numerous other publications were also considered, either related to methodologies for risk assessment or for the description of mechanisms and their modelling.

**Table 5.** List of all selected indicators and the related effects

| Types of effects | Selected indicators | Associated Effects | Final Impacting Phenomenon |
|---|---|---|---|
| **Physical effects** | $CO_2$ stream density | Storage volume | Reduced storage capacity |
| | | Compression work and pipe strength | Increased energy and cost |
| | Interfacial tension | Storage volume | Increased storage capacity |
| **Chemical effects** | Corrosiveness | Steel pipe corrosion | Increased probability of a sudden leakage of gas at surface |
| | Acidity of the stream | Cement (well) porosity and integrity (leakage pathway) | Increased probability of emanation of gas at surface + contamination of aquifer |
| | | Caprock porosity and integrity (leakage pathway) | Increased probability of emanation of gas at surface + contamination of aquifer |
| **Tox/excotox effects** | Toxic effects | Acute toxic effect | Increased severity in case of a sudden leakage of gas at surface |
| | | Chronic toxic effect (e.g. drinking water) | Increased severity in case of contamination of an aquifer |
| | Ecotoxic and long-term effects | Chronic ecotoxic effect (e.g. aquifer or near-surface) | Increased severity in case of contamination of an aquifer or emanation of gas at surface |

In order to perform a global assessment a semi-quantitative approach was chosen which is very common in risk analysis and is especially recommended when there is a need to compare a large range of phenomena. For each selected indicator a scoring scale ranging from 0 to 4 was proposed. For each impurity a score of 4 on each indicator is associated with an un-acceptable level of risk or consequence (or un-acceptable effect), defined by threshold values from regulation or from literature. The lower scores are then deduced, either with

linear scales (e.g. $CO_2$ stream density) or logarithmic scales (e.g. toxic effects). Essentially, level 0 is dedicated to absence of effect or negligible effect e.g. when the impurity concentration is below the level of detection.

The result for a whole $CO_2$ stream is the sum of the results for individual impurities. The 6 indicators are then displayed (see examples on figure 27 for two different $CO_2$ streams, as identified in Task 1 of the project). The final interpretation of the results for different capture processes is presently being performed. These 6 scores can also be summed up in order to give a global "impact index" which can in turn be combined with other social or economic criteria e.g. in a cost-benefit analysis. If necessary the requirements from such a global analysis may induce us to refine the choice of relevant indicators and scoring scales.
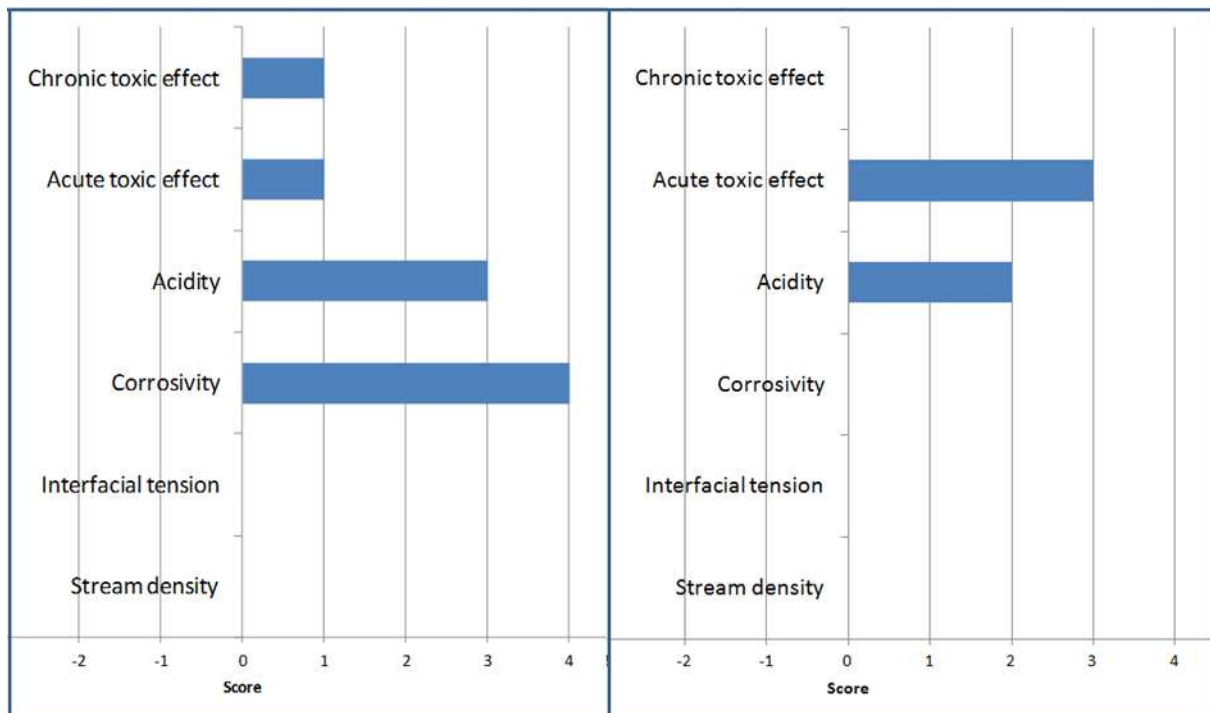


**Figure 27.** Display of scores for the 6 indicators for a $CO_2$ stream (left: a hypothetical post-combustion stream, global impact index = 9; right: a hypothetical high-purity $CO_2$ after pre-combustion, global impact index = 5).

# 8. CONCLUSIONS

Based on a comprehensive realistic-scale experimental test programme complemented with state-of-the-art mathematical modelling, the $CO_2$QUEST project has conducted a techno-economic assessment of $CO_2$ purity captured from fossil fuel power plants and industrial emission sources on its transport and storage. WP1 provided a cornerstone to the project in two main ways. First, a literature review was conducted to establish the range and level of impurities present in streams arising from the power sector and industrial $CO_2$ capture technologies. A cost-benefit analysis to assess the effect of $CO_2$ capture scenario selection on overall process costs and the $CO_2$ product purity was also performed. Secondly, in WP1 the development of methods and Equations of State (EoS) capable of predicting the phase equilibria, thermodynamic and transport properties of $CO_2$ mixtures under the wide range of fluid conditions likely to be encountered in the CCS chain was undertaken. Also in this WP EoS development was supported by numerous experiments undertaken to establish the thermophysical properties of $CO_2$ mixtures, including tertiary and quaternary mixtures, at the typical pressures and temperatures in CCS processes.

The focus of WP2 was on the fluid flow of $CO_2$ mixtures during "normal" CCS operations and during accidental high pressure releases of $CO_2$ following pipeline rupture in brittle or ductile fracture modes. At the same time, the impact of $CO_2$ impurities on the compression power requirements using various $CO_2$ compression strategies was investigated via the application of EoS. Additionally, the EoS have been coupled to a CFD code to simulate steady-state fluid flow within pipeline networks.

In order to provide understanding of the types of phenomenon that can occur during a high pressure $CO_2$ release and to provide validation data for the associated CFD simulations, $CO_2$ mixture experimental releases at various scales have been performed. Medium-scale controlled release experiments of $CO_2$ mixtures have been conducted in order to establish a better understanding of the influence of impurities on both the flow inside the pipe and on the external dispersion. Large-scale releases with pure and impure $CO_2$ were also performed using a purpose built and highly instrumented pipeline in Dalian, China, including on full bore releases. Also in WP2, CFD models have been developed and used to simulate impure $CO_2$ releases following puncture or rupture of a $CO_2$ pipeline. The models have incorporated EoS in order to fully account for the phase-equilibrium impacts induced by the presence of

impurities and in turn validated by comparing the results to those from the dispersion experiments conducted during the project. Investigations of three different steel materials for CCS pipelines have also been conducted to establish their response to impurities such as $H_2S$ on corrosion as well as brittle and ductile fracture behaviour. The latter involved the development of the state-of-the-art fluid/structure interaction fracture models ultimately enabling the selection of pipeline materials properties required in order to resist long running catastrophic fractures.

WP3 was devoted to developing the understanding of the impact of impurities in the subsurface during geological storage of $CO_2$. To this end experiments were conducted to investigate the effect of impure $CO_2$ injection into the subsurface. Shallow aquifer $CO_2$ /impurities injection experiments conducted by INERIS in France have concluded that there is no significant impact of $CO_2$ impurities on aquifer contamination.

Meanwhile, the deep well $CO_2$ injection test experiments performed in Heletz, Israel have helped to define standard operating procedures for $CO_2$ injection. The geochemical impact of impure $CO_2$ on storage reservoir integrity in a deep saline aquifer has also been studied through modelling. A radially 2D model was constructed to simulate the relevant reactive transport models focussing on the impact of $SO_2$ on the brine-rock system in sandstone, showing the acidic and reactive properties of this impurity.

WP4 focussed on full-chain techno-economic analyses of CCS networks, including detailed process system simulations of different options for $CO_2$ purification from oxyfuel combustion and post-combustion capture technologies. The different product purities for the different $CO_2$ capture technologies were taken into consideration in $CO_2$ transport network modelling via the blending of $CO_2$ streams to achieve a final trunk line with a $CO_2$ stream of composition suitable for subsurface injection. Finally, the optimised overall CAPEX and OPEX of the full chain system was derived for the anticipated ranges of $CO_2$ purity for the different sources. WP5 analysed the downstream impacts of $CO_2$ impurities on pipeline transport and geological storage by classifying impurity impacts into physical, chemical and toxic and by developing a point scoring mechanism to describe their severity.

In conclusion, the $CO_2QUEST$ project has provided the fundamentally important knowledge and tools needed to define the $CO_2$ impurity tolerance levels, mixing protocols and control

measures for pipeline networks and storage infrastructure, thus contributing to the development of relevant standards for the safe design and economic operation of CCS.

# 9. Acknowledgments

# 10. References

Ahmad, M., Gernert, J., & Wilbers, E., 2014. Effect of impurities in captured $CO_2$ on liquid–vapor equilibrium. Fluid Phase Equilibr. 363, 149–155.

Birkholzer, J.T., Zhou, Q., Tsang, C.F., 2009. Large-scale impact of $CO_2$ storage in deep saline aquifers: a sensitivity study on the pressure response in stratified systems. Int. J. Greenhouse Gas Control 3(2), 181–194.

Brown, S., Mahgerefteh, H., Martynov, S., Sundara, V., Mac Dowell, N., 2015. A multi-source flow model for CCS pipeline transportation networks. Int. J. Greenh. Gas Control 43, 108–114.

Brown S., Mahgerefteh, H., Martynov, S., Sundara, V., Mac Dowell, N. 2015. A multi-source flow model for CCS pipeline transportation networks. Int. J. Greenhouse Gas Control 43, 108–14.

Chapoy, A., Nazeri, M., Kapateh, M., Burgass, R., Coquelet, C., & Tohidi, B., 2013. Effect of impurities on thermophysical properties and phase behaviour of a $CO_2$-rich system in CCS. Int. J. Greenh. Gas Control 19, 92–100.

Chickos, J.S., 2005. Heat of sublimation data. In NIST chemistry Webbook; Linstrom, P. Mallard, W.G.; NIST Standard Reference Database Number 69; National Institute of Standards and Technology: Gaithersburg, MD, June 2005; Toluene.

$CO_2$PipeHaz, 2009. Quantitative failure consequence hazard assessment for next generation $CO_2$ pipelines: The missing link. Accessed 11/11/14; [$CO_2$PipeHaz Project Website]. Available from: http://www.co2pipehaz.eu/.

$CO_2$QUEST, 2013. Impact of the Quality of $CO_2$ on Storage and Transport, $CO_2$QUEST Project Website. http://www.co2quest.eu/ (accessed: 01.07.14).

Cole, I.S., Corrigan, P., Sim, S., Birbilis, N., 2011. Corrosion of pipelines used for $CO_2$ transport in CCS: is it a real problem? Int. J. Greenh. Gas Control 5, 749–756.

Condor, J., Unatrakarn, D., Wilson, M. Asghari, K., 2011. A Comparative Analysis of Risk Assessment Methodologies for the Geologic Storage of Carbon Dioxide. Energy Procedia 4, 4036-4043.

Davis, J.A., Rodewald, N., Kurata, F., 1962. Solid-liquid-vapor phase behavior of the methane-carbon dioxide system. AIChE Journal 8 (4), 537–539.

de Visser, E., Hendriks, C., Barrio, M., Mona, J., Mølnvik, M.J., de Koeijer, G. Liljemark, S., Le Gallo, Y., 2008. Dynamic CO2 quality recommendations. Int. J. Greenhouse Gas Control 2(4), 478–484.

Döbereiner, S.M. Thibaux P., 2013. Analysis of slant fracture in battelle drop weight tear tests. Proceedings of the 6th International Pipeline Technology Conference, Ostend, Belgium.

Dodds, K., Watson M., Wright I., 2011. Evaluation of risk assessment methodologies using the In Salah $CO_2$ storage project as a case history. Energy Procedia 4, 4162–4169.

Duan, Z., Mao, S., 2006. A thermodynamic model for calculating methane solubility, density and gas phase composition of methane-bearing aqueous fluids from 273 to 523K and from 1 to 2000bar. Geochim. Cosmochim. Ac. 70(13), 3369–3386.

Duan, Z., Sun, R., Liu, R., Zhu. C., 2007. An accurate thermodynamic model for the calculation of $H_2S$ solubility in pure water and brines. Energ. Fuel 21(4), 2056–2065.

Edlmann, K., Niemi, A., Bensabat, J., Haszeldine, R.S., McDermott, C.I., 2016. Mineralogical properties of the caprock and reservoir sandstone of the Heletz field scale experimental $CO_2$ injection site, Israel; and their initial sensitivity to $CO_2$ injection. Int. J. Greenh. Gas Control. in press.

Fagerlund, F., Niemi, A., 2007. A partially coupled fraction-by-fraction modelling approach to the subsurface migration of gasoline spills. J. Contam. Hydrol. 89, 174–198.

Fagerlund, F., Niemi, A., Bensabat, J., Shtivelman, V., 2013. Design of a two-well field test to determine in situ residual and dissolution trapping of $CO_2$ applied to the Heletz $CO_2$ injection site. Int. J. Greenhouse Gas Control 19, 642–651.

Fandiño, O., Trusler, J.P.M., Vega-Maza, D., 2015. Phase behavior of $(CO_2 + H_2)$ and $(CO_2 + N_2)$ at temperatures between (218.15 and 303.15) K at pressures up to 15 MPa. Int. J. Greenh. Gas Control 36, 78–92.

Farret, R., Manceau, J-C., Le Gallo, Y., Neuville, N., 2011a. Note de synthèse Tâche 2.2: Identification de scénarios de risques de référence pour un complexe de stockage de $CO_2$, Convention n° 1094C0003 Ademe-GEOGREEN.

Farret, R., André, L., Brosse, E., Broutin, P., Chopin, F., Gombert, P., Jallais, S., Saysset, S., 2012. Substances Annexes au $CO_2$ pour un Stockage Souterrain (SACSS) - Rapport du Groupe de Travail du Club $CO_2$, réf. INERIS-DRS-12-127545-07346A Farret et al, SACCS.

HYSYS, 2014. Documentation: Aspen HYSYS Simulation basis. AspenTech, USA.

Jäger, A., Span, R., 2012. Equation of State for Solid Carbon Dioxide Based on the Gibbs Free Energy. J. Chem. Eng. Data, 57 (2), 590–597.

Jamois, D., Proust, C., Hebrard, J., 2014. Hardware and instrumentation to investigate massive spills of dense phase $CO_2$. Chem. Eng. Trans. 36, 601–606.

Kunz, O., Klimeck, R., Wagner, W.,Jaeschke, M., 2007. The GERG-2004 Wide-Range Equation of State for Natural Gases and Other Mixtures, GERG Technical Monograph 15, Fortschr.-Ber. VDI, Reihe 6, Nr. 557, VDI Verlag, Düsseldorf.

Mahgerefteh, H., Brown, S., 2011. Influence of Line Pressure and Temperature on Fracture Propagation Behaviour in $CO_2$ Pipelines, Rio Pipeline Conference and Exposition, Rio de Janeiro, Brazil, 20th-22nd September.

Mahgerefteh, H., Oke, A.O., Rykov, Y., 2006. Efficient numerical solution for highly transient flows. Chem. Eng. Sci. 61(15), 5049–5056.

Makino, H., Inoue, T., Endo, S., Kubo, T., Matsumoto, T., 2004. Simulation method for shear fracture propagation in natural gas transmission pipelines. Int. J. Offshore Polar Engineering 14, 60–68.

Martynov, S. Brown, S., 2014. $CO_2$QUEST Internal Report: A Report Describing the Optimum $CO_2$ Compression Strategy. Deliverable 2.2, University College London, UK.

Martynov, S., Mac Dowell, N., Brown, S., Mahgerefteh, H., 2015. Assessment of Integral Thermo-Hydraulic Models for Pipeline Transportation of Dense-Phase and Supercritical $CO_2$. Ind. Eng. Chem. Res. 54, 8587–8599.

Martynov, S., Brown, S., Mahgerefteh, H., Sundra, V., Chen, S., Zhang, Y., 2013. Modelling three-phase releases of carbon dioxide from high-pressure pipelines. Process Saf. Environ. 92(1), 36–46.

Mohitpour, M., Seevam, P., Botros, K.K., Rothwell, B., Ennis, C., 2011. Pipeline transportation of carbon dioxide containing impurities, ASME Press, New York, NY, USA.

Moore, J.J., Allison, T., Lerche, A., Pacheco, J., and Delgado, H. Development of Advanced Centrifugal Compressors and Pumps for Carbon Capture and Sequestration Applications. in The Fortieth Turbomachinery Symposium 2011, Houston, Texas 107–120.

Niemi, A. Bensabat, J, Shtivelman, V, Edlmann, K, Gouze, P., Luquot, L., Hingerl,F, Benson, S.M., Pezard, P.A, Rasmusson, K., Liang,T., Fagerlund, F., Gendler, M., Goldberg,I, Tatomir,A., Lange, T., Sauter, M., and Freifeld, B. (2016a) Heletz experimental site overview, characterization and data analysis for $CO_2$ injection and geological storage. Int. J. Greenhouse Gas Control, in press.

Niemi, A., Gouze, P., Bensabat, J., 2016b. Characterization of formation properties for geological storage of $CO_2$ - Experiences from the Heletz $CO_2$ injection site and other example sites from the EU FP7 project MUSTANG. Int. J. Greenhouse Gas Control, in press.

Oldenburg, C.M., 2008. Screening and Ranking Framework for geologic $CO_2$ storage site selection on the basis of health, safety and environmental risk. Environ. Geol. 54, 1687–1694.

Peng, D., Robinson, D.B., 1970. A new two-constant equation of state. 4th International Heat Transfer Conference, Paris, Heat Transfer 1970, volume VI, paper B.7.b.

Porter, R.T.J., Fairweather, M., Kolster, C., Mac Dowell, N., Shah, N., Woolley, R., (in prep.). CCS cost reduction potential through lower $CO_2$ purity levels. Int. J. Greenh. Gas Control, submitted.

Porter, R.T.J., Fairweather, M., Pourkashanian, M., Woolley, R.M., 2015. The range and level of impurities in $CO_2$ streams from different carbon capture sources. Int. J. Greenh. Gas Control 36, 161–174.

Posch, S., Haider, M., 2012. Optimization of $CO_2$ compression and purification units ($CO_2$CPU) for CCS power plants. Fuel 101, 254–263.

Prada, P., Konda, M., Shah, N., 2011. Development of an Integrated $CO_2$ Capture, transportation and Storage Infrastructure for the UK and North Sea using an Optimisation Framework. AIChe Annual Meeting, Minneapolis, October 17th 2011.

Pruess, K., 2004. The TOUGH codes - a family of simulation tools for multiphase flow and transport processes in permeable media. Vadose Zone Journal, 3(3), 738–746.

Pruess, K., Spycher, N., 2007. ECO2N – A fluid property module for the TOUGH2 code for studies of $CO_2$ storage in saline aquifers. Energ. Convers. Manage. 48(6), 1761–1767.

Rasmusson, K., Rasmusson, M., Fagerlund, F., Bensabat, J., Tsang, Y., Niemi, A., 2014. Analysis of alternative push-pull-test-designs for determining in-situ residual trapping of carbon dioxide. Int. J. Greenhouse Gas Control 27, 155–168.

Rebscher, D., Wolf, J. L., Jung, B., Bensabat, J., Segev, R., and Niemi, A. P., 2014. Effects of impurities in $CO_2$ spreading model development for field experiments in the framework of the $CO_2$QUEST Project, AGU Fall Meeting, Vol.1, H21A-0708, 2014.

Savage, D., Maul, P.R., Benbow, S., Walke, R.C., 2004. A generic FEP database for the assessment of long-term performance and safety of the geological storage of $CO_2$. Quintessa Report QRS-1060A-1.

Serpa, J., Morbee, J., Tzimas, E., 2011. Technical and Economic Characteristics of a $CO_2$ Transmission Pipeline Infrastructure, in, Joint Research Centre Institute for Energy, Petten.

Sim, S., Cole, I.S., Bocher, F., Corrigan, P., Gamage, R.P., Ukwattage, N., Birbilis, N., 2013. Investigating the effect of salt and acid impurities in supercritical $CO_2$ as relevant to the corrosion of carbon capture and storage pipelines. Int. J. Greenh. Gas Control 17, 534–541.

Span, R., Eckermann, T., Herrig, S., Hielscher, S., Jäger, A., Thol, M., 2015. TREND. Thermodynamic Reference and Engineering Data 2.0.1, Lehrstuhl fuer thermodynamik, Ruhr-Universitaet Bochum.

Talemi, H.R., Steinhoff, M., Cooreman S., Van den Abeele, F., Verleysen, P., 2016a. Effects of high strain rates on ductile slant fracture behaviour of pipeline steel: experiments and modelling. Proceedings of the 11th International Pipeline Conference (IPC2016), Calgary, Alberta, Canada.

Talemi, H.R., Cooreman S., Van Hoecke, D., 2016b. Finite element simulation of dynamic brittle fracture in pipeline steel: A XFEM-based cohesive zone approach. Proc. Inst. Mech. Eng., Part L.

Talemi, H.R., 2016. Numerical simulation of dynamic brittle fracture of pipeline steel subjected to DWTT using XFEM-based cohesive segment technique, Frattura ed Integritá Strutturale, accepted for publication.

Wang, J., Ryan, D., Anthony, E.J., Wigston, A., Basava-Reddi, L., Wildgust, N., 2012.The effect of impurities in oxyfuel flue gas on $CO_2$ storage capacity. Int. J. Greenh. Gas Control 11, 158–162.

Wareing, C.J., Woolley, R.M., Fairweather, M., Falle, S.A.E.G., 2013. A composite equation of state for the modeling of sonic carbon dioxide jets in carbon capture and storage Scenarios, AIChE J. 59, 3928–3942.

Wetenhall, B., Race, J.M., Downie, M.J., 2014. The effect of $CO_2$ purity on the development of pipeline networks for carbon capture and storage schemes. Int. J. Greenh. Gas Control 30, 197–211.

Wilday, J., Paltrinieri, N., Farret, R., Hebrard, J., Breedveld, L., 2011. Addressing emerging risks using carbon capture and storage as an example. Process Safety and Environmental Protection 89, 463–471.

Witkowski, A., Majkut, M., 2012. The Impact of $CO_2$ Compression Systems on the Compressor Power Required for a Pulverized Coal-fired Power Plant in Post-combustion Carbon Dioxide Sequestration. Archive Mech. Eng. 59(3), 343–360.

Wolf, J.L., Niemi, A., Bensabat, J., Rebscher, D. (in prep.). Benefits and restrictions of 2D reactive transport simulations of impurities co-injected with $CO_2$ in a saline aquifer, Int. J. Greenhouse Gas Control, in preparation.

Woolley, R.M., Fairweather, M., Wareing, C.J., Proust, C., Hebrard, J. Jamois, D., Narasimhamurthy, V.D., Storvik, I.E., Skjold, T., Falle, S.A.E.G., Brown, S., Mahgerefteh, H., Martynov, S., Gant, S.E., Tsangaris, D.M., Economou, I.G., Boulougouris, G.C., Diamantonis, N.I., 2014. An integrated, multi-scale modelling approach for the simulation of multiphase dispersion from accidental $CO_2$ pipeline releases in realistic terrain. Int. J. Greenh. Gas Control 27, 221–238.

Woolley, R.M., Fairweather, M., Wareing, C.J., Falle, S.A.E.G., Proust, C., Hebrard, J., Jamois, D., 2013. Experimental measurement and Reynolds-averaged Navier–Stokes modelling of the near-field structure of multi-phase $CO_2$ jet releases, Int. J. Greenhouse Gas Control 18, 139–149.

Woolley, R.M., Fairweather, M., Wareing, C.J., Proust, C., Hebrard, J., Jamois, D., Narasimhamurthy, V.D., Storvik, I.E., Skjold, T., Falle, S.A.E.G., Brown, S., Mahgerefteh, H., Martynov, S., Gant, S.E., Tsangaris, D.M., Economou, I.G., Boulougouris, G.C., Diamantonis, N.I., 2014. An integrated, multi-scale modelling approach for the simulation of

multiphase dispersion from accidental $CO_2$ pipeline releases in realistic terrain, Int. J. Greenhouse Gas Control 27, 221–238.

Xu, T., Sonnenthal, E., Spycher, N., Zheng, L., 2014. TOUGHREACT V3.0-OMP Reference Manual: A Parallel Simulation Program for Non-Isothermal Multiphase Geochemical Reactive Transport, LBNL-DRAFT. - Lawrence Berkeley National Laboratory, University of California, Berkeley.